https://doi.org/10.5194/gmd-2020-114
Preprint. Discussion started: 22 June 2020


Geoscientific Model Development Discussions
Open Access

# $i_N$RACM: Incorporating $^{15}N$ into the Regional Atmospheric Chemistry Mechanism (RACM) for assessing the role photochemistry plays in controlling the isotopic composition of $NO_x$, $NO_y$, and atmospheric nitrate.

Greg Michalsk[1], Huan Fang[1], Wendell W.Walters[2], and David Mase[1].

[1]*Purdue University, Department of Earth, Atmospheric, and Planetary Sciences, Department of Chemistry. West Lafayette, IN. USA*

[2]*Brown University, Institute for Environment and Society. Providence, RI. USA*

Correspondence: Greg Michalski, gmichals@purdue.edu

Key Points

- Modeling nitrogen isotope fractionation during the photochemical oxidation of nitrogen oxides into atmospheric nitrate.
- Incorporation of N isotopes of NOy into the Regional Atmospheric Chemistry Mechanism.
- Implications for quantifying $NO_x$ sources and oxidation pathways using nitrogen isotopes.

https://doi.org/10.5194/gmd-2020-114
Preprint. Discussion started: 22 June 2020


Geoscientific Model Development Discussions
Open Access


## Abstract

Nitrogen oxides, classified as $NO_x$ (nitric oxide (NO) + nitrogen dioxide ($NO_2$)) and $NO_y$ ($NO_x$ + $NO_3$, $N_2O_5$ $HNO_3$, + $HNO_4$ + HONO + Peroxyacetyl nitrate (PAN) + organic nitrates + any oxidized N compound), are important trace gases in the troposphere, which play an important role in the formation of ozone, particulate matter (PM), and secondary organic aerosols (SOA). Among many uncertainties in movement of atmospheric N compounds, nowadays understanding of $NO_y$ cycling is limited by $NO_x$ emission budget, unresolved issues within the heterogeneous uptake coefficients of $N_2O_5$, the formation of organic nitrates in urban forests, etc. A photochemical mechanism used to simulate tropospheric photochemistry was altered to include $^{15}N$ compounds and reactions as a means to simulate $\delta^{15}N$ values in $NO_y$ compounds. The 16 N compounds and 96 reactions involving N used in Regional Atmospheric Chemistry Mechanism (RACM) were replicated using $^{15}N$ in a new mechanism called $i_N$RACM. The 192 N reactions in $i_N$RACM were tested to see if isotope effects were relevant with respect to significantly changing the $\delta^{15}N$ values (+/- 1‰) of $NO_x$, HONO, and/or $HNO_3$. The isotope fractionation factors ($\alpha$) for relevant reactions were assigned based on recent experimental or calculated values. Each relevant reaction in the $i_N$RACM mechanism was tested individually and in concert in order to assess the controlling reactions. The final mechanism was tested by running simulations under different conditions that are typical of pristine, rural, urban, and highly polluted environments. The results of these simulations predicted several interesting $\delta^{15}N$ variations.

https://doi.org/10.5194/gmd-2020-114
Preprint. Discussion started: 22 June 2020




## 1. Introduction

Nitrogen oxides are an integral part of atmospheric chemistry, controlling the oxidation state of the troposphere, influencing aerosol formation, altering the pH of rainwater, and facilitating the movement of nitrogen through the N cycle. Nitrogen oxides are classified as $NO_x$ (nitric oxide (NO) + nitrogen dioxide ($NO_2$)) and $NO_y$ ($NO_x$ + $NO_3$, $N_2O_5$ $HNO_3$, + $HNO_4$ + HONO + Peroxyacetyl nitrate (PAN) + organic nitrates + any oxidized N compound) [*Day et al.*, 2003; *Harrison et al.*, 1999; *Hegglin et al.*, 2006; *Ma et al.*, 2013]. $NO_x$ produces ozone ($O_3$) through $NO_2$ photolysis, and NO acts as a catalyst in $O_3$ production when volatile organic compounds (VOCs) are present. In turn, $O_3$ photolysis generates OH radicals, which initiates a radical chain reaction involving $HO_2$ and organic peroxide propagators that result in the oxidation of chemically reduced compounds in the troposphere making them more soluble [*Finlayson-Pitts and Pitts*, 2000; *Seinfeld and Pandis*, 1998]. Thus, $NO_x$ facilitates the cleansing of the atmosphere through the production of $O_3$ and $OH_x$ (OH + $HO_2$), which together define the troposphere's oxidation state [*Bloss et al.*, 2005; *Lelieveld et al.*, 2008; *Prinn*, 2003]. These oxidants play an important role in the formation of particulate matter (PM) [*Bauer et al.*, 2007; *Pye et al.*, 2010], forming secondary organic aerosols (SOA) via VOC oxidation [*Hoyle et al.*, 2011; *Shrivastava et al.*, 2017]. They also generate secondary inorganic PM through $NO_x$, sulfur oxides ($SO_x$), and ammonia ($NH_3$) neutralization, which leads to ammonium nitrate ($NH_4NO_3$) and ammonium sulfate ($(NH_4)_2SO_4$) production [*Cao et al.*, 2017; *Pan et al.*, 2018; *Pusede et al.*, 2016]. The production of PM has important consequences for air quality aerosols [*Andreae and Crutzen*, 1997], human health [*Bruningfann and Kaneene*, 1993; *Hall et al.*, 1992], and radiative forcing [*Charlson et al.*, 1992; *Chen et al.*, 2007]. Termination reactions in $NO_y$ cycling produces $HNO_3$, and facilitates the production of sulfuric acid ($H_2SO_4$), two strong acids that decrease the pH of rain, known colloquially as acid rain and impact aerosol pH, both of which triggers a number of negative impacts on the environment [*Brimblecombe et al.*, 2007; *Lajtha and Jones*, 2013]. When $NO_y$ is deposited to the surface by wet and dry deposition, it transfers bioavailable N to ecosystems that may be bereft of, or saturated with, bioavailable N. This process can shift the balance of both terrestrial and aquatic ecosystems and impact the goods and services that those ecosystems can normally deliver [*Du et al.*, 2019; *E. M. Elliott et al.*, 2019; *Fowler et al.*, 2013]. Thus, understanding $NO_y$ sources and their chemistry is important for an array of scientific disciplines and evaluating their social, economic, and cultural impact on the environment.

Despite this importance, there are numerous knowledge gaps in the understanding of the cycling of $NO_y$ in the atmosphere. The $NO_x$ emission budget is still poorly constrained. Most emission inventories rely on fixed emission factors for some sources that may, in fact, be variable. For example, power plant $NO_x$ emissions are based on assumed efficiency of catalytic converters that may not be accurate [*Srivastava et al., 2005; Felix et al., 2012*]. Soil NO emissions are highly dependent on soils moisture, redox conditions, fertilizer application rates, type, and timing making them challenging to constrain [*Shepherd, 1991; Galloway et al., 2004; Hudman et al., 2012; Houlton et al., 2013; Pilegaard, 2013*]. There are several unresolved issues with the heterogeneous uptake coefficients of $N_2O_5$ [*Brown et al.*, 2001; *Brown et al.*, 2006; *Chang et al.*, 2011] and the formation of organic nitrates in urban forests [*Lee et al., 2016; Romer et al., 2016; Kastler and Ballschmiter*, 1998]. The relative importance and mechanism of HONO formation versus HONO emissions are also hotly debated. Likewise, reactions of $NO_y$ in

https://doi.org/10.5194/gmd-2020-114
Preprint. Discussion started: 22 June 2020



the aqueous phase and mixed aerosols are not fully understood. Chemical transport models (CTMs) do not accurately predict aerosol nitrate concentrations or other $NO_y$ mixing ratios [*Spak and Holloway*, 2009; *Zhang et al.*, 2009]. Therefore, it is important that these uncertainties in $NO_y$ cycling be resolved if we aim to have accurate air quality forecast and accurate chemistry-climate models that use CTMs.

It has been suggested that stable N isotopes can provide clues as to the origin of $NO_x$ [*Elliott et al.*, 2009; *Felix and Elliott*, 2014;*Walters et al.*, 2015b] and the oxidation pathways that transform in $NO_y$ [*Walters and Michalski*, 2015; 2016]. Isotopic measurements of $NO_y$ compounds show a wide range of $\delta^{15}N$ values (Eq. (1)), which has been suggested to indicate variability in $NO_x$ emission sources, chemical processing, and/or a combination of these effects. $\delta^{15}N$ is defined by the relative difference between the $^{15}N/^{14}N$ ratio in a $NO_y$ compound and the ratio in air $N_2$ (the arbitrary reference compound) and is typically reported in parts per thousand e.g. per mil (‰)

$$\delta^{15}N_{NOy}\,(‰) = [(^{15}NO_y/^{14}NO_y) / (^{15}N_2/^{14}N_2) - 1]*1000 \qquad \text{Eq. (1)}$$

A number of studies have measured the $\delta^{15}N$ values of $NO_x$ collected from $NO_x$ sources such as power plants [*Felix et al.*, 2012], automobiles [*Walters et al.*, 2015a], biomass burning [*Fibiger and Hastings*, 2016], and non-road sources [*Felix and Elliott*, 2014].

Many studies have measured the $\delta^{15}N$ values of various $NO_y$ compounds collected from the troposphere. Most of the $NO_y$ $\delta^{15}N$ data is for nitrate that has been collected on filters ($PM_{2.5}$, $PM_{10}$, TSP) [*Moore, 1977; Savard et al., 2017*], as the dissolved $NO_3^-$ anion in rain [*Heaton, 1987; Hastings et al., 2003; Felix et al., 2015; Yu & Elliott, 2017*], or as gas phase $HNO_3$ [*Elliott et al., 2009; Savard et al., 2017*]. The range of tropospheric $NO_y$ $\delta^{15}N$ values span -50 to +15‰ but the average is ~0‰. Two hypotheses have been offered to explain these ranges: Source and Photochemistry. The source hypothesis [*Elliott et al., 2007; Hastings et al., 2013*] suggesting that the tropospheric $NO_y$ $\delta^{15}N$ value range reflects the spatial and temporal mixing of $NO_x$ sources with different $\delta^{15}N$ values that is then converted into $NO_y$. The photochemistry hypothesis [*Freyer*, 1978; *Freyer et al.*, 1993; *Walters et al.*, 2018] suggests that the observed $NO_y$ $\delta^{15}N$ variations arise via isotope effects occurring when photochemical cycling partitions N into the myriad of $NO_y$ compounds. These two hypotheses are not mutually exclusive. Indeed it is likely to be a combination of both processes, but their relative importance likely shifts depending on environmental conditions such as a region's $NO_x$ source diversity, plume versus dispersed chemistry, photolysis intensity, and oxidant load. In turn, the $\delta^{15}N$ data might be a new key to reconciling some of the current uncertainties in $NO_y$ sources and chemistry, if it can be properly interpreted.

What has become clear is that the temporal-spatial heterogeneity of $NO_x$ sources and the complex photochemistry of $NO_y$ presents a serious challenge to deciphering the observed $NO_y$ $\delta^{15}N$ values. Except for a few isolated cases, a proper assessment of $NO_y$ $\delta^{15}N$ values will require incorporating isotope effects into 3-D chemical transport models. This will include emission modeling of $^{15}NO_x$, meteorological mixing, factoring in isotope effects during $NO_y$ removal processes, and developing chemical mechanisms that incorporate $^{15}N$ compounds and their relative rate constants. Here we take the first step in this endeavor by developing a chemical mechanism (0-D photochemical box model) that explicitly includes $^{15}NO_y$ compounds and the isotope effects that occur during their cycling through photolysis, equilibrium, and kinetic reactions.

https://doi.org/10.5194/gmd-2020-114
Preprint. Discussion started: 22 June 2020




# 2. Methods

## 2.1 Chemical and isotopic compounds and reactions included in $i_N$RACM

The basis of the $i_N$RACM model is incorporating $^{15}N$ into the Regional Atmospheric Chemistry Mechanism (RACM) detailed in Stockwell et al. [*Stockwell et al.*, 1997]. RACM is an extension of the chemical mechanism used in the Regional Acid Deposition Model (RADM2) [*Stockwell et al.*, *1990*], but with updated inorganic and organic chemistry. There are 17 stable inorganic compounds, 4 inorganic intermediates, 32 stable organic compounds, including 4 biogenic organics, and 24 organic intermediates in the RACM mechanism. The RACM mechanism uses 237 chemical reactions, including 23 photolysis reactions *[Atkinson, 1990;Atkinson et al., 1992*]. The rate constants, photolysis cross-sections and quantum yields for the inorganic compounds were taken from [*DeMore et al.*, *1994*]. The RACM mechanism aggregates the thousands of VOC in the atmosphere into 16 anthropogenic and 3 biogenic organic compounds. Part of the aggregation criteria is based on the reactivity of a VOC towards the hydroxyl radical (•OH). Full details on how •OH reacts with alkanes, alkenes, aromatics, and other VOCs, and the aggregation rationale, can be found in Stockwell et al. (*1997*). The actinic flux model used in RACM was developed by Madronich (*1987*) and calculates the wavelength-dependent photon flux as a function of solar zenith angle, which is a function of time (hourly), date, latitude, and longitude. Inputs to the model include temperature, water vapor content, pressure, initial gas mixing ratios and primary pollutant emission rates. Complete details on the RACM mechanism can be found in Stockwell et al. (1997). The numerical solver used was VODE, part of the ODEPACK, a commonly used, and validated, collection of initial value ordinary differential equation solvers [*Brown et al.*, 1989; *Hindmarsh*, 1983].

Our $i_N$RACM (isotope N in RACM) mechanism was generated by adding $^{15}N$ isotopologues for the 2 primary (NO, $NO_2$) and the 11 secondary N pollutants found in the original RACM mechanism (Table S1a). By definition, an isotopologue is a compound with the same chemical formula but a different mass (e.g. NO = 30 amu and $^{15}NO$ = 31 amu, with N = $^{14}N$). This is different from isotopomers, which are isotopic isomers, compounds with the same mass but a different structure caused by isotopic substitution (e.g. $^{15}NNO_5$ = 109 amu and $N^{15}NO_5$ = 109 amu). Of all the reactive N compounds only $N_2O_5$ has multiple possible $^{15}N$ substitutions and 2 isotopologues were defined in the $i_N$RACM: $^{15}NNO_5$ and $^{15}N^{15}NO_5$. The $^{15}N$ compounds are numbered (Table S1a) and subscripted (a, b) in order to maintain a compound numbering scheme that is consistent with that in Stockwell et al. (*1997*). The non-N compounds found in both RACM and $i_N$RACM mechanisms have been excluded from Table S1a for the sake of brevity but can be found in Stockwell et al. (*1997*). The 16 $^{15}N$ compounds (Table S1a) were added to the original RACM FORTRAN code provided by Stockwell by using Z =$^{15}N$ (e.g. $^{15}NO$ is defined as ZO).

The 96 chemical reactions involving N compounds (Table S2a-f) were inspected and replicated for $^{15}N$ based on classification as the reaction being either "N only" or "multiple N" reactions. Single N reactions are those where only one N compound was found in the products and reactants, for example $NO + O_3 \rightarrow NO_2+O_2$. Multiple N reactions could have multiple N compounds in the reactants, the products, or both. Examples of these possible multiple N reactions are $NO_2+NO_3 \rightarrow N_2O_5$, $N_2O_5 \rightarrow NO_2 + NO_3$, and $NO_3 + NO \rightarrow NO_2 + NO_2$ respectively. For these multiple N reactions, a reaction probability was factored into the isotopologue/isotopomer rate constants (discussed below). For example, the N

https://doi.org/10.5194/gmd-2020-114
Preprint. Discussion started: 22 June 2020



isotopologue/isotopomer equivalent of the $N_2O_5 \rightarrow NO_2 + NO_3$ reaction has two isotopomer reactions: $^{15}NNO_5 \rightarrow {}^{15}NO_2 + NO_3$ and $^{15}NNO_5 \rightarrow NO_2 + {}^{15}NO_3$. These two isotopologue rate constants (R54a, R54b) are multiplied by a factor of 1/2 to account for this statistical probability. Similar statistical factors were considered when N compounds or intermediates decomposed or reacted to form multiple N products (R52a, R52b, R52c, R52d). All N isotopologue reaction stoichiometry is given in Table S2a-f.

## 2.2 Isotope effects included in $i_N$RACM

The main challenge for developing realistic isotopologue chemistry in $i_N$RACM is quantifying the differences in rate constants caused by isotopic substitution. These isotope effects can be classified into four general types: Equilibrium isotope effects (EIE), kinetic isotope effects (KIE), photo-induced isotope fractionation effects (PHIFE), and vapor pressure isotope effects (VPIE). For this study, the most up-to-date isotope fractionations were used when establishing the framework for modeling their effect associated with $NO_x$ oxidation chemistry. The established framework will easily enable an adjustment of isotope effects as we improve our understanding of isotope fractionation factors.

Urey *(1947)* and Bigelesien and Mayer *(1947)* showed that EIEs are driven by the sensitivity of molecular and condensed-phase vibrational frequencies to isotopic substitutions [*Bigeleisen and Mayer*, *1947; Urey, 1947*]. Because vibrations are used in the molecular partition function (Q) to calculate equilibrium constants, isotopic substitution results in isotopologues having different equilibrium constants. Urey [*1947*] defined the reduced partition function ratio for two isotopologues of the same compound as a β value. For example, the reduced partition function ratio of nitric oxide N isotopologues is $Q_{15NO}/Q_{NO} = \beta_{NO}$, with the heavy isotope placed in the numerator by convention. The ratio of two β values is denoted as $\alpha_{\beta1/\beta2}$ the isotope fractionation factor. For example, $\alpha_{NO/NO2}$ is the temperature-dependent isotope fractionation factor (EIE) for the $NO + {}^{15}NO_2 \leftrightarrow {}^{15}NO + NO_2$. In this case, at 298K $\beta_{NO}$ = 1.0669 and $\beta_{NO2}$ = 1.1064 and $\alpha_{NO/NO2} = \beta_{NO}/\beta_{NO2}$ = 0.9643 [*Walters and Michalski, 2015*].

A KIE is the relative change in the rate of a unidirectional chemical reaction when one of the atoms of the reactants is substituted with an isotope [*Bigeleisen and Wolfsberg*, *1958*]. KIEs are driven by the change in energy required to proceed over the reaction barrier (transition state) as well as changes in the probability of quantum mechanical tunneling [*Wolfsberg et* al., *2010*]. This generally results in a lighter isotopologue reacting faster than a heavier isotopologue. Much of the early research on KIEs were investigations of the KIE in reactions containing hydrogen isotopes and these studies usually defined a KIE = $k_L/k_H = \alpha_{L/H}$, where the k's are the rate constants for the light and heavy isotopologues. This is the inverse of the definition of α usually used in research dealing with EIE, VPIE, PHIFE and this inversion can lead to confusion. In this paper, in order to maintain consistency between the α values for EIE, KIE, VPIE, and PHIFE, α will be defined as heavy/light for all four effects.

The α values for EIE and KIE can be determined using a number of approaches. The α values for EIE can be calculated if molecular constants (e.g. harmonic frequencies and anharmonicity constants) of the isotopologue pair are known. Accurate molecular constants are difficult to accurately measure for large molecules and as a result, they primary exist only for diatomic and triatomic isotopologues [*Richet et al.*, *1977*]. The only experimental EIE values for $^{15}N$ isotopologues of $NO_y$ is for the EIE between NO and $NO_2$ [*Sharma et al., 1970; Walters et al., 2016*]. To determine the EIE in other $NO_y$ compounds we must rely on quantum chemistry

https://doi.org/10.5194/gmd-2020-114
Preprint. Discussion started: 22 June 2020



computation methods to estimate the molecular constants and anharmonicity constants. Recent works utilizing these methods have estimated the EIE for most non-organic $NO_y$ compounds [*Walters and Michalski*, *2015*]. For KIE, in addition to molecular constants, the transition state vibrational frequencies are also needed. The only $^{15}N$ KIE calculation to date for an $NO_y$ compound is for the KIE for the NO + $O_3$ reaction [*Walters and Michalski*, *2016*].

These EIE and KIE values have been incorporated in $i_N$RACM in this study Table S2a-c. If there is no isotope effect associated with any of the $NO_y$ reactions, then α is set equal to 1. The $^{15}N$ isotopologue rate constant for any reaction is then $\alpha^{14}k$ where $^{14}k$ is the rate constant for any $^{14}N$ reaction in RACM and these are given in Table S2a-f. It is useful to define the magnitude of EIE and KIE in the same per mil (‰) notation used to quantify a $\delta^{15}N$ values by defining an enrichment factor ε(‰) = (α-1)1000. For example, the $NO_x$ isotope exchange equilibrium mentioned above, the $\varepsilon_{NO/NO2}$ = -35.7‰. This means that $^{15}NO/NO$ ratio would be 35.7‰ smaller than the $^{15}NO_2/NO_2$ ratio if the isotopes in two gases were statistically distributed (Table S2b).

PHIFE is the relative change in photolysis rates of isotopologues due to the substitution of a heavier isotope [*Yung and Miller, 1997*]. In the atmospheric N cycle, $NO_2$, $NO_3$, $N_2O_5$, and HONO readily undergo photolysis at wavelengths of light that penetrate into the troposphere. The PHIFE can be estimated using a simple zero-point energy shift model (ΔZPE). In this approximation, the absorption spectra of the heavier isotopologue is generated by applying a uniform blue shift (equal to ΔZPE) to the measured spectral absorbance of the light (major) isotopologue [*Blake et al.*, *2003; Liang et al., 2004; Miller and Yung, 2000]*. This results in isotopic fractionation because the wavelength (λ) dependent photolysis rate constant (J(λ)) is dependent on the convolution of the absorption cross-section (σ(λ)), actinic flux (F(λ)), and quantum yield (ϕ(λ)) (Eq. (2)):

$$^{x}J(\lambda) = {}^{x}\sigma(\lambda)F(\lambda)\phi(\lambda) \quad \text{Eq. (2)}$$

The overall photolysis rate constant ($^{z}J$) can be calculated by integrating σ, F, and ϕ over a range of wavelengths that can cause dissociation ($\lambda_1$ and $\lambda_2$):

$$^{x}J = \int_{\lambda_1}^{\lambda_2} {}^{x}\sigma(\lambda)F(\lambda)\phi(\lambda)d\lambda \quad \text{Eq. (3)}$$

The N isotopologue fractionation (α) resulting from photolysis (of $NO_2$ isotopologues) is calculated by (Eq. (4)).

$$\alpha_{47/46} = \frac{^{47}J}{^{46}J} \quad \text{Eq. (4)}$$

It is important to note that there are limitations in the ΔZPE-shift model [*Blake et al., 2003; Liang et al., 2004; Miller and Yung, 2000]*. These include the failure to account for changes in shape and intensity of absorption spectra upon isotopic substitution and the same quantum yield (as a function of wavelength) is assumed for all isotopologues. Despite these limitations, this approach should still give a rough estimate of photolytic fractionation until experimentally determined PHIFE's become available [*Blake et al.*, 2003; *Liang et al.*, 2004; *Miller and Yung*, 2000].

Isotopologues partition differently between phases giving rise to the VPIE. This is most notable in gas-liquid systems [*Van Hook et al.*, 2001], but also can occur in gas-solid equilibrium.

https://doi.org/10.5194/gmd-2020-114
Preprint. Discussion started: 22 June 2020



Both of these may ultimately be important for understanding $\delta^{15}N$ variability in $NO_y$ compounds. For example, solid-gas VPIE may be relevant for the $HNO_{3(g)} + NH_{3(g)} \leftrightarrow NH_4NO_{3(s)}$ reaction, whose temperature-dependent equilibrium can shift dramatically diurnally [*Morino et al., 2006*] and seasonally [*Paulot et al., 2016*]. It is likely that this VPIE will result in the particle phase $NO_3^-$ having a different $\delta^{15}N$ value compared to the gas phase $HNO_3$ [Heaton, 1987]. Additionally, possible VPIE occurring during wet and dry deposition, such as $HNO_{3(g)} \rightarrow HNO_{3(aq)}$ may be relevant for $\delta^{15}N$ variations $NO_3^-$ in precipitation *[Freyer et al., 1993]*. Multiphase reactions are not included in RACM since it is only concerned with gas phase reactions. These effects may be important for accurate $\delta^{15}N$ predictions and should be addressed in more complex models, but this is a limitation in any "gas phase only" photochemical box model. Similarly, $NO_y$ aqueous phase reactions, such as $2NO_2 + H_2O \rightarrow HNO_3 + HNO_2$, are not included in RACM, which may limit $i_N$RACM's ability to accurately predict the $\delta^{15}N$ values of dissolved $NO_3^-$ in rainfall samples.

## 2.3 Sensitivity analysis: Determining the "reaction relevance" of $NO_y$ isotopologues

The objective of the $i_N$RACM model is to make predictions about the temporal and spatial variation of $\delta^{15}N$ value in various N compounds caused by EIE, KIE, and PHIFE, and compare them to observations. Currently, the $\delta^{15}N$ observations are largely limited to $HNO_3$, as either particulate or dissolved $NO_3^-$, but there are a few recent measurements of the $\delta^{15}N$ values of $NO_x$ [*Walters et al., 2018*] and HONO [*Chai and Hastings, 2018*]. The $\delta^{15}N$ values of organic nitrates and PAN may be made in the not so distant future, but there is no published data to date. Thus, a given isotopologue reaction pair in $i_N$RACM was considered "relevant" if it significantly changed the $\delta^{15}N$ value (±1‰) of $NO_x$, HONO, or $HNO_3$. This relevance was determined by conducting a sensitivity analysis on the PHIFE, KIE, and EIE effects for all N reactions. This was done by arbitrarily setting $\alpha = 0.98$ ($\varepsilon = -20‰$) for one isotopologue reaction and $\alpha = 1.0$ for all others, then running a test case. This test case is a 5-day simulation, beginning at 3 AM on March 1 (2007) and simulates mid-latitude suburban chemistry using the trace gas and meteorology parameters given in Table S3a-b. This simulation was repeated 96 times until every N containing reaction was tested. For example, $NO_x$, HONO, or $HNO_3$ $\delta^{15}N$ values are not sensitive to R51 (Fig. 1). The following section discusses which $i_N$RACM reactions are relevant and the approaches used to determine the appropriate $\alpha$ values for those reactions. Testing for isotope mass balance was also performed by hourly summing all N isotopologues, excluding

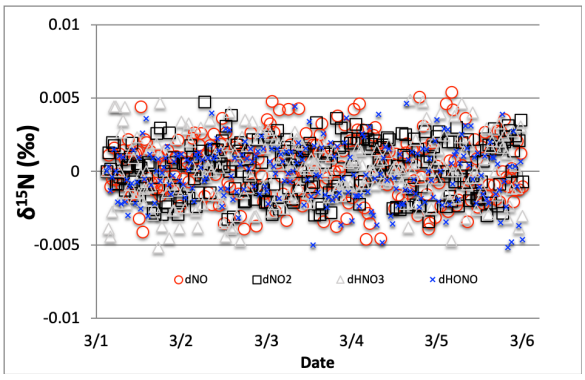


Figure 1. The time evolution of $\delta^{15}N$ values of NO, $NO_2$, HONO, and $HNO_3$, caused by the $NO_3 + NO \rightarrow NO_2 + NO_2$ reaction (R 51, $51_a$). This reaction only induces a $\delta^{15}N$ variation of +/- 0.005‰ in the relevant compounds. Thus, this reaction is considered irrelevant and $i_N$RACM sets R51a $\alpha = 1.0$.

https://doi.org/10.5194/gmd-2020-114
Preprint. Discussion started: 22 June 2020

Geoscientific Model Development Discussions
Open Access

unreactive $N_2$. Over the course of a five day simulation the total $\delta^{15}N$ value averaged 0.023 ± 0.048‰, with most of the variance occurring during the initial four hour model spin-up. Excluding these data points the total $\delta^{15}N$ value averaged 0.018 ± 0.016‰, demonstrating limited impact of rounding errors and effective isotope mass conservation.

### 2.3.1 PHIFE relevant in the $i_N$RACM mechanism

Only one of the 6 photolysis reactions involving N compounds was found to be relevant. $NO_2$ photolysis (R1) had a significant impact on the $\delta^{15}N$ value of $NO_x$, HONO, and $HNO_3$ (Fig. 2). The initial difference between the $\delta^{15}N$ of NO and $NO_2$ values is roughly equal to the arbitrarily set -20‰ enrichment factor. The nature of the diurnal oscillation in $\delta^{15}N$ values on the three relevant $NO_y$ compounds and the dampening effect over time will be discussed in the results section.

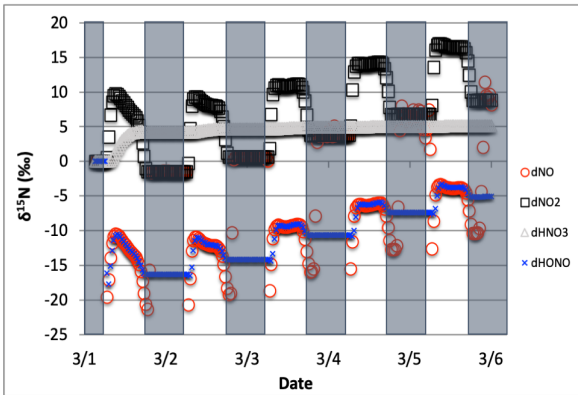


Figure 2. The time evolution of $\delta^{15}N$ values of NO, $NO_2$, $HNO_3$, and HONO caused by PHIFE during $NO_2$ photolysis.

When there is sufficient photolysis of any single $NO_y$ compound, then the $\delta^{15}N$ value of that compound tends to significantly change, but often neither the $HNO_3$, HONO, nor $NO_x$ $\delta^{15}N$ values are affected. For example, the arbitrary α for $NO_3$ photolysis (R7 and R8) alters the $\delta^{15}N$ value of $HNO_3$ and $NO_x$ by less than 0.1‰ (not shown), but it induces a large diurnal changes in the $\delta^{15}N$ value of $NO_3$ and $N_2O_5$, with sharp transitions occurring during sunrise and sunset (Fig. 3). This is easily understood. For our test case, during the day $^{15}NO_3$ would be left behind because $^{14}NO_3$ is preferentially being photolyzed. The daytime $N_2O_5$ formed from this $NO_3$ (positive $\delta^{15}N$) and $NO_2$ ($\delta^{15}N \sim 0$) thus has a $\delta^{15}N$ values halfway between these two reactants (isotope mass balance). However, there is so little $NO_3$ and $N_2O_5$ during the day that essentially no $HNO_3$ is being formed through these precursors and the $NO_3$ PHIFE is not manifested in the $NO_x$ or $HNO_3$ $\delta^{15}N$ value. During the night, photolysis and the PHIFE ceases and any $NO_3$ and $N_2O_5$ formed by $NO_2$ oxidation have $\delta^{15}N$ values equal to the $NO_2$.

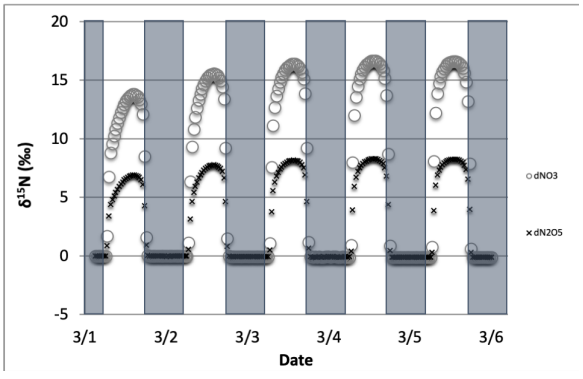


Figure 3. The time evolution of $\delta^{15}N$ values of $NO_3$, and $N_2O_5$ caused by PHIFE during $NO_3$ photolysis.

$NO_x$, HONO, and $HNO_3$ are not sensitive to the other $NO_y$ photolysis reactions because of this isotope mass balance effect.

$$\delta^{15}N_{NOy} = \Sigma f_{NOyi} \bullet \delta^{15}N_{NOyi} \quad \text{Eq. (5)}$$

Where $f_{NOyi}$ is the mole fraction of any $NO_{yi}$ compound relative to total $NO_y$, $\delta^{15}N_{NOyi}$ is

https://doi.org/10.5194/gmd-2020-114
Preprint. Discussion started: 22 June 2020



the $\delta^{15}N$ value of that compound, and $\delta^{15}N_{NOy}$ is the value of total N, which in these simulations is arbitrarily set to 0‰. For an ε = -20‰ and a threshold of "importance" set to ± 1‰, isotope mass balance requires that $f_{NOyi}$>0.05. Only NO, $NO_2$, HONO, and $HNO_3$ compounds meet this threshold (Fig. 4). All other $f_{NOyi}$ values are an order of magnitude smaller, the largest being $f_{HNO4}$ and it only reaches a maximum value of 0.005. By the end of the second simulation day the $f_{HNO3}$ has approached 1 and effectively minimizes the other $f_{NOyi}$ values because it is the only stable N compound because the other $NO_y$ compounds are very photochemically active. If we exclude this build up in $HNO_3$ from the sum of $NO_y$, then $f_{NO}$, and $f_{NO2}$ (and HONO during some hours, see discussion) become the dominant fractions (Fig. 4) and they control the other $f_{NOyi}$. Even under this constraint, the $f_{HNO4}$ only reaches 0.001 (Fig. 4). Thus, in $i_N$RACM, the α values of $\alpha_{R4}$- $\alpha_{R8}$ were set equal to 1 and only the $\alpha_{R1}$ was assigned a non-1 value, which was determined using a PHIFE theory (discussed below).

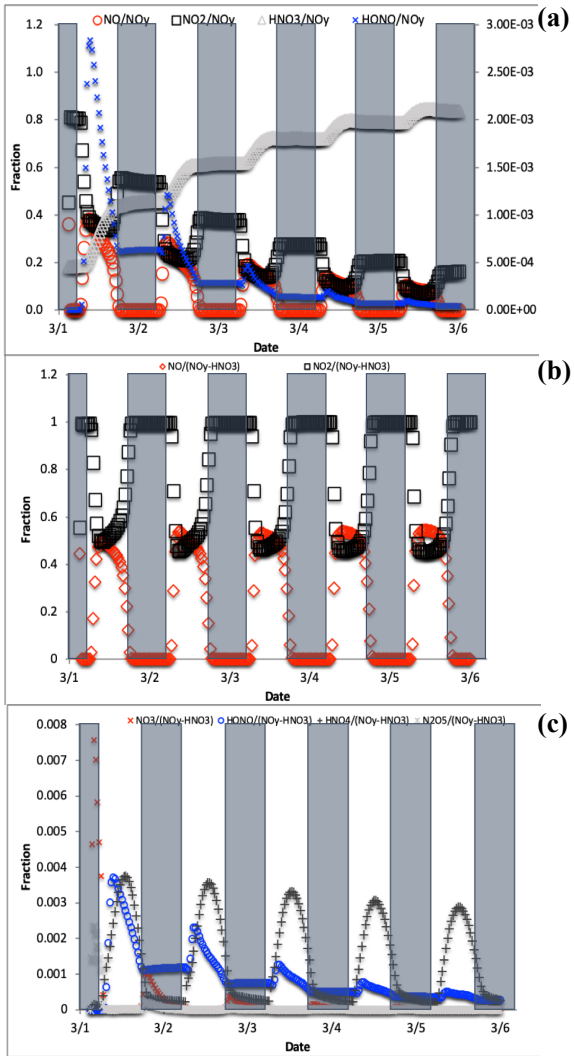


Figure 4. The change in $f_{NO}$, $f_{NO2}$, $f_{NO3}$, and $f_{HONO}$ (right axis) over the 5-day simulation shows the transition from $NO_y$ as mostly $NO_x$ to predominately $HNO_3$ (top, a). For reactive $NO_y$ ($NO_y$ – $HNO_3$) large diurnal changes in $f_{NO}$ and $f_{NO2}$ (middle, b) caused by photolysis minimize the other $f_{NOy}$ values, none of which exceeds 0.01 (bottom, c).

### 2.3.2 KIE relevant in $i_N$RACM mechanism

The KIE for 12 N containing compounds and their 96 reactions were evaluated using the same sensitivity analysis. The vast majority of reactions had little influence on the $\delta^{15}N$ values of $NO_x$, HONO, and $HNO_3$ (Fig. 1). Similar to the photolysis sensitivity, either reaction proximity or isotope mass balance were controlling $\delta^{15}N$ relevance. For example, $NO_2$ + OH is reaction that directly produces a significant fraction of $HNO_3$ and therefore R39 is relevant in the $i_N$RACM mechanism. In contrast, R95 produces very little $HNO_3$ so it has a negligible influence on the predicted $HNO_3$ $\delta^{15}N$ value. Therefore, the only relevant KIE reactions that have α ≠ 1 in $i_N$RACM mechanism are R39, R91-R97, R48 (Table S2b).

https://doi.org/10.5194/gmd-2020-114
Preprint. Discussion started: 22 June 2020




2.3.3 EIE relevant in $i_N$RACM mechanism

While some EIE are naturally handled in the $i_N$RACM mechanism, such as the $NO_2$–$NO_3$–$N_2O_5$ equilibrium, other potentially important N isotope exchange reactions are not directly expressed in RACM and must be considered. From a thermodynamic perspective, the EIE for any two N containing compounds can be calculated. The rate at which these compounds can achieve equilibrium, however, needs careful consideration. For example, the EIE for the isotope exchange reaction NO + $^{15}HNO_3$ ←→ $^{15}NO$ + $HNO_3$ has been calculated and measured [*Brown and Begun, 1959]*. Yet, steric considerations would suggest it would be very improbable for a gas phase reaction pathway or transition state to exist where two O atoms and a hydrogen from a $HNO_3$ could quickly migrate to a NO molecule during a collision. The result is that isotope exchange for this gas phase reaction is likely kinetically too slow to be relevant but is valid in a highly concentrated liquid phase [*Brown and Begun, 1959]*. The larger the N containing molecule the more difficult it is to envision gas phase EIE occurring on a timescale comparable to the residence time tropospheric N of about a week. On the other hand, the isotope exchange reaction NO + $^{15}NO_2$ ←→ $^{15}NO$ + $NO_2$ rapidly occurs [*Sharma et al.*, 1970] because it can form an ONONO ($N_2O_3$) stable intermediate. As such, $i_N$RACM only considers N isotope equilibrium between NO, $NO_2$, $NO_3$, and $N_2O_5$. Since the latter 3 compounds are already *chemically* equilibrated in RACM, they are by default isotopically equilibrated in $i_N$RACM. Therefore, the only new isotope exchange reaction added to $i_N$RACM was NO + $^{15}NO_2$ ←→ $^{15}NO$ + $NO_2$ (R238, R238a).

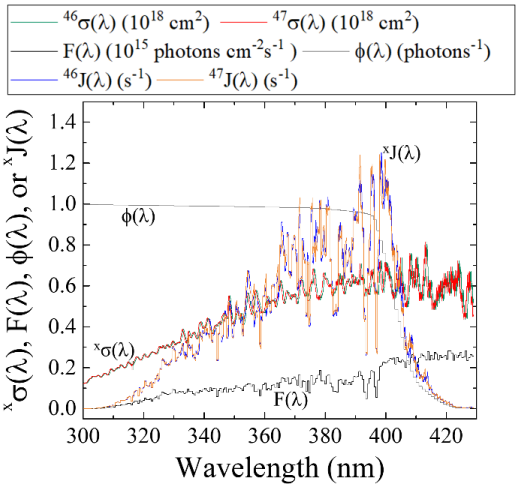


Figure 5. Literature reported $^{46}\sigma(\lambda)$ [*Vandaele et al.*, *2002*] F(λ) (at SZA of 60°; TUV model), and $NO_2$ ϕ(λ) [*Roehl et al.*, *1994*] and calculated $^{47}\sigma(\lambda)$ derived from the ZPE shift model for wavelengths relevant for tropospheric conditions for $NO_2$ photolysis. From these parameters, both $^{46}J(\lambda)$ and $^{47}J(\lambda)$ have been calculated (Eq. (2)).

## 2.4 Isotopologue fraction factors (α) used in $i_N$RACM

In this section we discuss the methodology used to determine the values for the relevant PHIFE, KIE, and EIE. These are reactions R1, R39, R48, R91-R97, and R238.

2.4.1 PHIFE derived α used in the $i_N$RACM mechanism

The PHIFE for R1 was calculated using existing $NO_2$ experimental photolysis cross-section of $^{14}NO_2$ for tropospheric relevant wavelengths (300 to 450 nm) [*Vandaele et* al., 2002]. Using the experimentally determined ΔZPE for the $^{15}NO_2$ isotopologue of 29.79 cm$^{-1}$ [*Michalski et al.*, *2004*], the $^{47}\sigma(\lambda)$ was blue shifted by roughly 0.3 nm from the experimentally measured

https://doi.org/10.5194/gmd-2020-114
Preprint. Discussion started: 22 June 2020



$^{46}\sigma(\lambda)$ [*Vandaele et al., 2002*] (Fig. 5). The wavelength dependent actinic flux, F(λ), was taken from the TUV model (NCAR) for solar zenith angles from 0 to 90° in 15° increments. The ϕ(λ) values were taken from experimental data at 298 K [*Roehl et al.*, *1994*], and it was assumed that there is no significant quantum yield isotope effect. Based on these assumptions the $^{46}J(\lambda)$ and $^{47}J(\lambda)$ values were calculated (Fig. 5). An important feature of $NO_2$ the wavelength dependent J include a peak near 390-400 nm that subsequently decreases at longer wavelengths until $NO_2$ photolysis ceases beyond 420 nm due to a $\phi = 0$ beyond this wavelength [*Roehl et al.*, *1994*]. Overall, the $NO_2$ PHIFE α value was found to be consistent for the wide range of solar zenith angles, ranging between 1.002 to 1.0042 with higher values occurring at lower solar zenith angles. We used an $\alpha = 1.0042$ for daylight hours.

2.4.2 KIE derived α used in the $i_N$RACM mechanism

2.4.2.1 KIE for the NO + $O_3$ reaction

The $^{15}\alpha_{48}$ for the reaction NO + $O_3$ → $NO_2$ +$O_2$ reaction was determined by *ab initio* calculations [*Walters and Michalski*, *2016*]. Generally, in a normal KIE the heavy $^{15}NO$ would react with $O_3$ slower than the light $^{14}NO$, which consistent with the calculated effect, however, it is relatively small (ε = -6.7‰ at 298 K). The $^{15}\alpha_{48}$ was determined to have the following temperature dependent relationship [*Walters and Michalski*, 2016] over the temperature range of 220 to 320 K (Eq. (6)):

$$\alpha_{48} = (0.9822*\exp(3.3523/T) \qquad \text{Eq. (6)}$$

2.4.2.2 KIE for the $NO_3$ + VOC reactions

The most influential reactions that impacted the $\delta^{15}N$ of $HNO_3$ were the three reaction pathways that generate $HNO_3$. This is because the isotope effect associated with this last step is largely retained in the product $HNO_3$ because photolysis of $HNO_3$ back into photochemically active compounds that could re-scramble N isotopes is slow, effectively "locking in" these final isotope effects. Two gas phase reactions groups are important for $HNO_3$ production. Nitric acid is produced mainly by R39 during the daytime [*Seinfeld and Pandis, 1998*] but this reaction is treated as an EIE as discussed below in the EIE section. During the nighttime, when the photolysis sink for $NO_3$ vanishes, $NO_3$ can react with VOCs to form $HNO_3$ via hydrogen abstraction reactions [*Atkinson*, *2000*]. Any individual $NO_3$ + VOC reaction had a small "relevance" for the $\delta^{15}N$ values of $NO_x$, and $HNO_3$, but given there are 7 such reactions (R91-R97) their sum may be important.

The KIE for each of the $NO_3$ +VOC→ $HNO_3$ reaction (R91-R97) was determined by assuming collisional frequency was the key KIE factor in such reactions. In these reactions (R91-R97) $NO_3$ abstracts a hydrogen from a hydrocarbon, acting though a transition state involving the oxygen atoms in the nitrate radical C--H--$ONO_2$. Since N is not directly participating in the bond formation it is classified as a secondary KIE [*Wolfsberg*, 1960]. Secondary KIE are typically much smaller than primary KIEs that occur at bond breaking/forming positions within a molecule [*Wolfsberg*, 1960]. Therefore, we assumed that the secondary KIE was negligible and did not factor into the α values for these 7 reactions. On the other hand, isotope substitution does change the relative rate of collisions for N isotopologues because of the change in molecular mass. The collisional frequency (Eq.7) for any of the $NO_3$ + VOC reaction pair was calculated assuming a hard sphere approximation via

https://doi.org/10.5194/gmd-2020-114
Preprint. Discussion started: 22 June 2020



$$A = \left[\frac{8kT}{\pi\mu}\right]^{1/2} \pi d^2 \qquad \text{Eq. (7)}$$

here μ is the reduced mass of either $NO_3$ or $^{15}NO_3$ and the specific hydrocarbon in a given reaction (R91-R97). When taking the isotopologue collision ratio, the constants, collision cross-section ($d^2$), and temperature cancel out giving a temperature independent KIE of

$$\alpha = \frac{k_{15}}{k_{14}} = \frac{A_{15}}{A_{14}} = \sqrt{\frac{\mu_{15}}{\mu_{14}}} \qquad \text{Eq. (8)}$$

The α for each $NO_3$ + VOC reaction (R91-R97) as calculated using the hydrocarbon mass (Table S1b) and the $NO_3$ isotopologue masses (62, 63 amu) and using Eq. (8).

2.4.3 EIE derived α used in the $i_N$RACM mechanism

2.4.3.1 EIE of NO + $NO_2$ exchange

The NO + $NO_2$ exchange was added to $i_N$RACM by defining a forward and reverse reaction (R238, R238a) and an equilibrium constant $K_{238} = k_{238}/k_{238a} = \alpha$. The forward rate constant ($k_{238}$) was based on the NO-$NO_2$ isotope exchange rate determined by Sharma et al. ($3.6*10^{14}$ $cm^3$ $s^{-1}$ $molecule^{-1}$). The reverse rate was calculated using $k_{238} = k_{238a}/\alpha_{238}$. The temperature-dependent for EIE of NO + $NO_2$ exchange (Eq. 9) was calculated using quantum mechanical techniques [*Walters and Michalski*, 2015] that matched well with recent experimental values [*Walters et al.*, 2016].

$$\alpha_{238} = 0.9771*\exp(18.467/T) \qquad \text{Eq. (9)}$$

2.4.3.2 EIE used in the $NO_2$ + OH reaction

The $^{15}\alpha_{39}$ for the $NO_2$+OH+M → $HNO_3$ reaction (R39) was determined by assuming equilibrium between $NO_2$ and $HNO_3$. The third body and the negative temperature dependence of the rate constant shows that, similar to $O_3$ formation, this reaction is an association reaction [*Golden and Smith, 2000*]. It proceeds through an excited intermediate, $*HNO_3$, that can undergo collisional deactivation by a third body M (Eq.10).

$$NO_2 + OH \xleftarrow{k_r} \xrightarrow{k_f} *HNO_3 \xrightarrow{k_d} HNO_3 \qquad \text{Eq. (10)}$$

in which $k_f$ and $k_r$ are the forward and reverse rate constants for the association step and $k_d$ is the rate constant for collisional deactivation. The $HNO_3$ production rate constant is then $k_f k_d[M]/k_r = K_{eq}k_d[M]$. This general form can be used to write two isotopologue equilibrium constants K

$$K_{39} = [*HNO_3]/([NO_2][OH]) = k_{39f}/k_{39r} \qquad \text{Eq. (11)}$$
$$K_{39a} = [*H^{15}NO_3]/([^{15}NO_2][OH]) = k_{39af}/k_{39ar} \qquad \text{Eq. (12)}$$

Since •OH is not participating in the N isotope chemistry, these two EIE effectively reduces the isotope chemistry to the temperature dependent $^{15}N$ EIE

https://doi.org/10.5194/gmd-2020-114
Preprint. Discussion started: 22 June 2020



$^{15}NO_2 + {}^*HNO_3 \leftrightarrow NO_2 + {}^*H^{15}NO_3$ Eq. (13)

$K_{39a}/K_{39} = \alpha_{HNO3/NO2} = \beta_{HNO3}/\beta_{NO2}$ Eq. (14)

The fundamental vibration frequencies for $HNO_3$* were taken to be the same as ground state $HNO_3$, similar to RRKM theory approaches used to calculate the uni-molecular decay rate of $HNO_3$* [*Golden and Smith, 2000*]. The temperature-dependent $\beta_{HNO3}$ and $\beta_{NO2}$ values for this exchange were taken from [*Walters and Michalski*, *2015*]. Since the reaction has a negative activation energy and has a fairly rapid rate constant at 101 kPa, (1 x $10^{11}$ $cm^{-3}$ $s^{-1}$) and the isotope effect due to the collisional deactivation frequency (Eq. 7) is minimal (~2‰) compared to the equilibrium effect (~40‰), the deactivation rate constants $k_d$ were set equal ($k_{d14}/k_{d15}$=1). Setting $k_{r14}$= $k_{r15}$, and using the $\alpha_{HNO3/NO2}$ equilibrium value the $k_{39a}$ for the $^{15}NO_2$ + OH → $H^{15}NO_3$ reaction is

$K_{39a} = \alpha_{HNO3/NO2} (K_{39})$ Eq. (15)

The temperature dependence of $\alpha_{HNO3/NO2}$ is derived from the tables in [*Walters and Michalski*, 2015] and $\alpha_{39}$ is then:

$\alpha_{39} = (0.973*\exp(19.743/T)$ Eq. (16)

For typical tropospheric temperatures the $\alpha_{HNO3/NO2}$ 1.040 suggesting the $\delta^{15}N$ of $HNO_3$ produced by the $NO_2$ + OH reaction will be +40‰ relative to tropospheric $NO_2$. This α value is larger and opposite the sign of the $^{15}\alpha$ = 0.9971 assumed by Freyer et al. (*1993*). Freyer's α was approximated by the using reduced mass of the OH-$NO_2$ activated complex. There two problems with this approach. First, the activation complex's reduced mass approximation should be viewed in terms as the *decomposition* rate constant, not the product formation rate constant as assumed by Freyer, because transition state theory assumes equilibrium between the stable *reactants* and the transition state [*Bigeleisen and Wolfsberg*, 1958; *Wolfsberg et al.*, 2010]. In other words, Freyer's α = 0.9971 should indicate that the $^{15}NO_2$-OH decomposes more slowly than $^{14}NO_2$-OH and therefore more likely to form $HNO_3$ at +2.9‰ (not -2.9‰ determined in Freyer). Secondly, the reduced mass approximation of the complex pair ignores the thermodynamic contribution of the reactants and the vibrations in the transitions state other than the bond forming (imaginary) vibration. Our approach overcomes both of these assumptions and incorporates the temperature dependence of the EIE for this reaction.

2.4.3.3 EIE used in heterogeneous reactions of $N_2O_5$

During the nighttime, the heterogeneous $HNO_3$ formation pathway becomes important [*Chang et al., 2011; Dentener and Crutzen, 1993; Riemer et al., 2003*]. During the night, NO is nearly completely oxidized to $NO_2$ leading to the build-up of the $NO_3$ radical (R48), the formation of $N_2O_5$ (R53), and heterogeneous $N_2O_5$ hydrolysis becomes a major source of $HNO_3$ production (discussed below). This is particularly true in regions that have high $NO_x$ mixing ratios and large aerosol surface areas such as urban centers [*Chang et al., 2011; Riemer et al., 2003*]. In order to assess the $^{15}N$ partitioning of this reaction pathway, both EIE and KIE were considered.

https://doi.org/10.5194/gmd-2020-114
Preprint. Discussion started: 22 June 2020



It was assumed that the fractionation factor for the $N_2O_5 \rightarrow 2HNO_3$ reaction was mainly controlled by nighttime equilibrium between $N_2O_5$ and $NO_2/NO_3$ (R53, R54). When factoring the isotopologue dynamics, this equilibrium can be viewed as an EIE via

$$^{15}NO_2 + NO_3 \leftrightarrow O_2{}^{15}N\text{--}O\text{--}NO_2 \leftrightarrow NO_2 + {}^{15}NO_3 \qquad \text{Eq. (17)}$$

here $^{15}N_2O_5$ is represented as the transition state $O_2{}^{15}N\text{--}O\text{--}NO_2$ to highlight the relative ease of N isotope exchange via oxygen migration during $N_2O_5$ formation and decomposition. The symmetry of $^{15}NNO_5$ and $N^{15}NO_5$ is also why they were not treated as isotopomers since they are structurally identical.

The $N_2O_5$ equilibrium in the RACM model is dealt with as a forward reaction R53 ($k_{53}$) and a decomposition reaction R54 ($k_{54}$) that are derived from the measured equilibrium constant ($K_{53}$) = ($k_{53}/k_{54}$). In $i_N$RACM the $N_2O_5$ isotopologue has 2 formation pathways, with two forward rate constants ($k_{53\ a,b}$) and two decomposition rate constants ($k_{54\ a,b}$) that were used to write their respective equilibrium constants K

$$^{15}NO_2 + NO_3 \leftrightarrow {}^{15}NNO_5 \quad (K_{53a} = k_{53a}/k_{54a}) \quad \text{Eq. (18)}$$
$$NO_2 + {}^{15}NO_3 \leftrightarrow {}^{15}NNO_5 \quad (K_{53b} = k_{53b}/k_{54b}) \quad \text{Eq. (19)}$$

Dividing $K_{53a}$ and $K_{53b}$ by $K_{53}$ yields isotopologue product and reactant ratios that can be evaluated using $\beta(\alpha)$ values from Walters and Michalski (*2015*). These were used to determine the $\alpha$ value for the $N_2O_5$ isotopologue equilibrium, which are simply a function of the formation and decomposition rate constants and temperature

$$K_{53a}/K_{53} = ({}^{15}NNO_5/N_2O_5)(NO_2/{}^{15}NO_2)(NO_3/NO_3) = \beta_{N2O5}/\beta_{NO2}$$
$$= \alpha_{N2O5/NO2} = k_{53a}/k_{53} \times k_{54}/k_{54a} \qquad \text{Eq. (20)}$$
$$K_{53b}/K_{53} = ({}^{15}NNO_5/N_2O_5)(NO_3/{}^{15}NO_3)(NO_2/NO_2) = \beta_{N2O5}/\beta_{NO3}$$
$$= \alpha_{N2O5/NO3} = k_{53b}/k_{53} \times k_{54}/k_{54b} \qquad \text{Eq. (21)}$$

The $N_2O_5$ decomposition rate constants were arbitrarily set to be equal ($k_{54} = k_{54a} = k_{54b}$) and the decomposition rate constants were then derived using the temperature dependent $\alpha$ values

$$k_{53a} = k_{53}(\alpha_{N2O5/NO2})\ \alpha_{N2O5/NO2} = 1.0266\ (298\ K) \qquad \text{Eq. (22)}$$
$$k_{53b} = k_{53}(\alpha_{N2O5/NO3})\ \alpha_{N2O5/NO3} = 1.0309\ (298\ K) \qquad \text{Eq. (23)}$$

The $\alpha$ for doubly substituted $^{15}N_2O_5$ isotopologue was determined using $\alpha = \beta_{15N2O5}/\beta_{NO2}\beta_{NO3}$ and the value for $\beta_{15N2O5}$ (1.272) was approximated using the principle of the geometric mean [*Bigeleisen*, 1958; *Snyder et al.*, 1999], yielding a temperature independent $\alpha$ = 1.057. However, the $N_2O_5$ system is insensitive to this □ value because the low probability of a $^{15}N + {}^{15}N$ reaction ($1.5 \times 10^{-5}$) relative to a $^{14}N + {}^{15}N$ reaction ($4 \times 10^{-3}$), thus the small temperature dependence was also ignored.

Because RACM is a gas phase chemical mechanism, it does not include heterogeneous reactions of $N_2O_5$ on aerosols, which would limit $i_N$RACM to accurately predict the $\delta^{15}N$ values, particularly at night. Gas chemical mechanisms are often used in larger 1, 2, and 3-D chemical

https://doi.org/10.5194/gmd-2020-114
Preprint. Discussion started: 22 June 2020




transport models that usually also include aerosol modules that calculate heterogeneous chemistry using inputs from the gas phase chemical mechanism (i.e. $N_2O_5$ concentrations). However, if the objective is to use a 0-D chemical box model to simulate local chemistry the $N_2O_5$ heterogeneous hydrolysis will need to be included. $i_N$RACM was modified to use a first order rate constant to calculate $N_2O_5$ heterogeneous hydrolysis [*Yvon et al. 1996; Riemer et al., 2003*]. The rate constant is a function of $N_2O_5$ molecular speed (c), the $N_2O_5$ uptake coefficient (γ) and the aerosol surface area density S.

$$-dN_2O_5/dt = d0.5HNO_3/dt = k_{N2O5}[N_2O_5] = R239 \qquad k_{N2O5} = \tfrac{1}{4} c\, \gamma\, S \quad \text{Eq. (24)}$$

The $k_{N2O5}$ values were assessed based on the different pollutant loadings and emission scenarios (Fig. 6). The $k_{N2O5}$ was calculated as a function of γ *[Anttila et al, 2006; Bertram & Thornton. 2009; Davis et al., 2008; Riemer et al., 2003; Riemer et al., 2009]* and S *[Cai et al., 2018; Kuang et al., 2010; McMurry et al., 2005; Petäjä et al., 2009; Qi et al., 2015]* values that span clean to highly polluted environments. This range yielded $k_{N2O5}$ = 1, 0.1, and 0.01 for high, medium, and low polluted environments (Fig. 6).

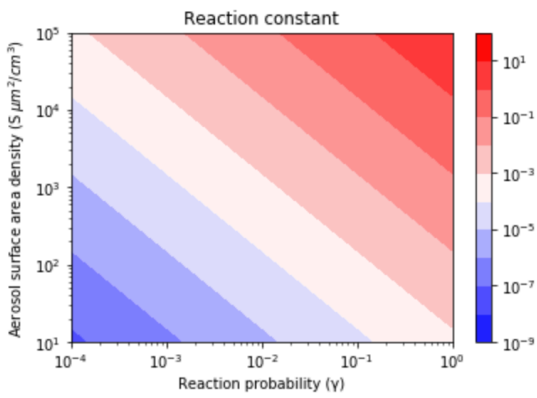


Figure 6. Contour lines of the same $k_{N2O5}$ values as a function of γ and S values. The γ values depend on aerosol composition and range from 3.8 x $10^{-5}$ (relatively dry sulfuric acid) to 1 (aqueous aerosol in the winter polar stratosphere). S values are a function of aerosol number density and size distribution and range from 52 (low scavenging rate, low particle growth rate) to 1140.1 (high scavenging rate, high particle growth rate).

Only the uptake coefficient (γ) and molecular speed (c) could have a KIE during aerosol uptake of $N_2O_5$ (R239, R239a, R239b). The γ term was ignored because *ab initio* work suggests that $N_2O_5$ hydrolysis activates through hydrogen bonding between water molecules on the aerosol surface and O atom in the $N_2O_5$ [*Snyder et al.*, 1999] making it a secondary (small) KIE for N. The c term is a function of the root of the $N_2O_5$ molecular mass and when the ratio is taken there is no temperature dependence yielding $\alpha_{239a} = (108/109)^{0.5} = 0.995$ and $\alpha_{239b} = (108/110)^{0.5} = 0.9909$.

An online interactive version of this $i_N$RACM model is available for public use at https://mygeohub.org/tools/sbox/

2.4.4 $i_N$RACM simulations

A number of $i_N$RACM simulations were run with two different purposes. The first set of simulations iteratively changed the α values from 1 to their values discussed above. These simulations aimed at investigating the importance of each α as they aggregated together. These include photolysis only, Leighton cycle, daytime chemistry, night-time chemistry, and full chemistry using the same test case (Table S3a-f). The second set of simulations replicated the

https://doi.org/10.5194/gmd-2020-114
Preprint. Discussion started: 22 June 2020



test case simulations (Table S4a-b, 5a-b) detailed in Stockwell (1997) and other pollution scenarios (Table S8). These were run with all α's activated but with varied initialized chemistry and primary pollutant emissions.

## 3.0 Results and Discussion

It is important to first test $i_N$RACM by turning on and off individual relevant isotope effects and then combining their cumulative effects. This is advantageous relative to simply running the full mechanism under different pollution scenarios because it would be a challenge to disentangle which isotope effects in the full mechanism were mainly responsible for $\delta^{15}N$ change in $NO_x$, HONO, or $HNO_3$ without such a systematic investigation. For example, it is likely that the $\delta^{15}N$ value of $NO_2$ will be a significant factor in the $\delta^{15}N$ value of $HNO_3$ because it is the reactant in R39 and R239. Thus, understanding which isotope effects control the $\delta^{15}N$ of $NO_2$ helps with interpreting the $\delta^{15}N$ value of $HNO_3$ and vice versa. Thus, this discussion section is divided into 3 sections. The first is the examination of the relevant isotope effects occurring during daytime photochemistry and their impact on $NO_x$, HONO, and $HNO_3$ $\delta^{15}N$ values. Secondly, is the examination of the relevant isotope effects occurring during nighttime chemistry (EIE and KIE) and their effect on $NO_x$, HONO, and $HNO_3$ $\delta^{15}N$ values. These first two discussion sections focus mainly on the relative importance of each isotope effect when the photochemical conditions are constant. Finally, the full $i_N$RACM mechanism will be tested under different atmospheric conditions such as variations in trace gas concentrations, aerosol loading, and hours of sunlight. This tests how changes in photochemical oxidation pathways results in difference in the $\delta^{15}N$ values of $NO_x$, HONO, and $HNO_3$.

### 3.1 The $\delta^{15}N$ of $NO_x$, HONO, and $HNO_3$ due to daytime chemistry

The role that daytime chemistry plays in determining the $\delta^{15}N$ values of $NO_x$, HONO, and $HNO_3$ was investigated by iteratively adding relevant fractionation factors to $i_N$RACM. The sensitivity of $NO_x$, HONO, and $HNO_3$ $\delta^{15}N$ values to $NO_2$ photolysis (R1a) was tested. The initial trace gas concentrations and emissions were set to the March 1 test cases (Table S3 a-f) and simulations were run with, and without, NO emissions. All subsequent test simulations will also use the March 1 test case in order to have a consistent comparison of $\delta^{15}N$ values between different simulations. It is noted that the initial $HNO_3$ and $O_3$ mixing ratios are set to zero and that the start time of the simulations is 3 a.m. The main daytime only effects will be $NO_2$ photolysis (R1), $O_3$ oxidation (R8) and reaction OH (R39) since both photolysis and OH chemistry is only relevant during the daytime. However, $NO_x$ isotope exchange and NO + $O_3$ will also play a vital role despite no being exclusively daytime reactions.

#### 3.1.1 The $\delta^{15}N$ values of $NO_x$, HONO, and $HNO_3$ due to the photolysis only

https://doi.org/10.5194/gmd-2020-114
Preprint. Discussion started: 22 June 2020




The simulations with only R1 isotope effect activated (with $NO_x$ emissions) shows a clear diurnal cycle in $NO_x$ and HONO $\delta^{15}N$ values and a weekly trend moving towards an approximate steady-state for $HNO_3$ $\delta^{15}N$ values, which can be explained by the PHIFE (Fig. 7a). Initially all $NO_y$ has $\delta^{15}N$ of zero (by default) and there is no photolysis at 3 am. At sunrise the $\delta^{15}N$ value of $NO_2$ goes negative and NO value positive since $^{15}NO_2$ is preferentially photolyzed ($\alpha_{R1}$ = 1.0042). The difference between the $\delta^{15}N$ values of NO and $NO_2$ ($\Delta\delta^{15}N_{NO\text{-}NO2}$ = $\delta^{15}N$ NO - $\delta^{15}N$ $NO_2$) at all times during the day is 4‰, which is the $\varepsilon_{R1a}$ value. During the night both the NO and $NO_2$ $\delta^{15}N$ values approach 0‰ because most NO is oxidized to $NO_2$ and NO emissions (0‰) dominate the NO nighttime budget (relative to residual day NO). Over the weeklong simulation, the $NO_x$ $\delta^{15}N$ value slowly increases by about one per mil. This is because $^{15}N$ depleted $NO_2$ is converted into $HNO_3$ leaving the residual $NO_x$ $^{15}N$ enriched. This is also the reason for the $\delta^{15}N$ values of $HNO_3$ that initially mimic the daytime $NO_2$ values and trends towards 0‰ by the end of the simulation week. The $\delta^{15}N$ values of HONO mimics the NO values during the daytime since the main reaction pathway forming HONO is OH + NO, which peaks in the morning (~10:00). HONO retains the evening $\delta^{15}N$ values through the night since most of the HONO is destroyed in the afternoon via photolysis and again follows NO $\delta^{15}N$ the next morning as its production again reaches a maximum (Fig. 7).

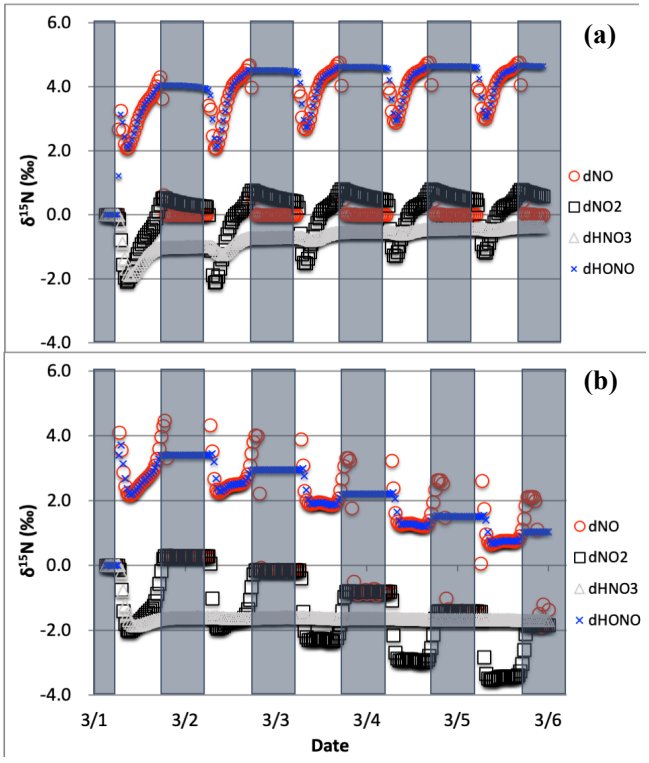


Figure 7. The $\delta^{15}N$ values of NO (O), $NO_2$, (☐) HONO (x), and $HNO_3$ (Δ) with only the photolysis isotope fractionations active. The 5-day simulation was under the conditions list in Table S3a-b. The gray boxes span night hours and the white span daytime. The top (a) is the simulation with $NO_x$ emissions and the bottom (b) is without $NO_x$ emissions.

The simulation without NO emissions shows a similar behavior but with some clear differences relative to the emission case. The $NO_x$ and HONO $\delta^{15}N$ values exhibit the same diurnal $\Delta\delta^{15}N_{NO\text{-}NO2}$ = 4‰ value. Unlike the emission case, however, the diurnal $NO_x$ $\delta^{15}N$ value peaks and troughs trend downward during the week-long simulation, with NO approaching 0‰ and $NO_2$ approaching -4‰. The $HNO_3$ $\delta^{15}N$ values reach roughly a steady state value of -1.7‰ after about a day and $NO_x$ is ~ -1.8‰ (Fig. 7b). This difference between the emission and non-emission case is a consequence of isotope mass balance ($f_x$ = mole fraction of compound x relative to total $NO_y$).

https://doi.org/10.5194/gmd-2020-114
Preprint. Discussion started: 22 June 2020



$$\delta^{15}N_{total} = 0 = f_{NOx} \bullet \delta^{15}N_{NOx} + f_{HNO3} \bullet \delta^{15}N_{NHNO3} + f_{ONIT} \bullet \delta^{15}N_{ONIT} \qquad \text{Eq. (25)}$$

The positive $\delta^{15}N$ $NO_y$ compound that effectively offsets the -1.7‰ in $HNO_3$ and -1.8‰ in $NO_x$ is organic nitrate that is +2‰ and makes about half the $NO_y$ pool and is roughly equal to $HNO_3$ + $NO_x$ ($f_{NOx}$ = 0.11, $f_{HNO3}$= 0.36, $f_{ONIT}$ = 0.53). In the $NO_x$ emission case only about 5% of $NO_y$ is as organic nitrate ($f_{NOx}$ = 0.17, $f_{HNO3}$= 0.78, $f_{ONIT}$ = 0.05) indicating a shift in oxidation pathways when NO and VOCs are emitted during the simulation relative to when they are not. In the emissions case the $NO_x$ mixing ratios at the end of the simulation are actually slightly higher than their initial ratios, in contrast to the no $NO_x$ emission case where 90% of $NO_x$ has been lost via oxidization into organic nitrate and $HNO_3$. This loss of N in the no emission scenario effectively shuts down the oxidation chemistry. For example, the day 5 mixing ratio of $O_3$ is 45 $ppb_v$ (reasonable) for the emission case but only 2 $ppb_v$ for the non-emission case (unreasonable). Therefore, we exclude no-emission simulations for the chemistry analysis discussed in this section and restrict them to the no emission simulations to 48 hours in the final test case analysis (See section 4).

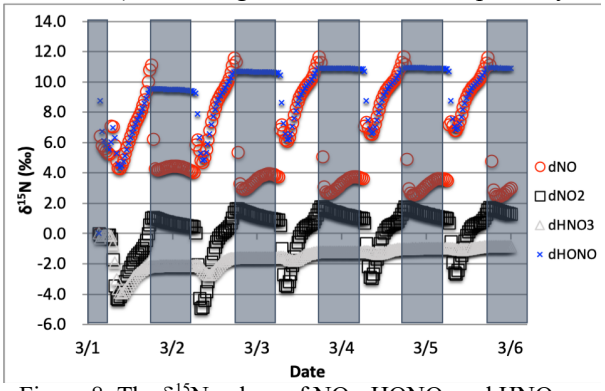


Figure 8. The $\delta^{15}N$ values of $NO_x$, HONO, and $HNO_3$ when isotope effects associated R1 and R48 are combined, with $NO_x$ emission. The 5-day simulation was under the conditions list in Table S3a-b. The diurnal patterns are reflecting the relative importance of photolysis and $O_3$ chemistry during the day and night.

### 3.1.2 The $\delta^{15}N$ values of $NO_x$, HONO, and $HNO_3$ due to the combined Leighton cycle

The simulations with both $NO_2$ photolysis (R1) and $O_3$ + NO (R48) isotope effects active shows similar diurnal and weekly trends as the photolysis only simulations, they are just slightly amplified (Fig. 8). The daytime $\Delta\delta^{15}N_{NO\text{-}NO2}$ is now ~ 9.5‰, which is close to the additive of the two isotope effects ($\varepsilon_{48a}$ = -6.7‰, $\varepsilon_{R1a}$ = 4.2‰). This is logical since $^{15}NO$ is reacting with $O_3$ slower than $^{14}NO$, preferentially leaving behind $^{15}NO$ and thus the higher NO $\delta^{15}N$ value. The $HNO_3$ $\delta^{15}N$ values reach the mean of the daytime $NO_2$ $\delta^{15}N$ values via the $NO_2$ + OH reaction. The slight (1‰) upward trend of $NO_x$ and $HNO_3$ are due to isotope mass balance as detailed in the photolysis only case. Similar to the photolysis only case the $\delta^{15}N$ of HONO is mimicking daytime NO $\delta^{15}N$ values.

### 3.1.3 The $\delta^{15}N$ values of $NO_x$, HONO, and $HNO_3$ due to the combined Leighton cycle and $NO_x$ isotope exchange

The $\delta^{15}N$ values of $NO_x$ produced when both the Leighton cycle and $NO_x$ isotope exchange are active exhibit a very dynamic diurnal range that is a function of the $NO_x$ mixing ratios. At high $NO_x$ mixing ratios (150 ppb, 1/3 NO, 2/3 $NO_2$, Fig. 9a) the $\Delta\delta^{15}N_{NO\text{-}NO2}$ is -40‰ at night as expected for $NO_x$ isotopic equilibrium ($\varepsilon_{NO/NO2}$ = -40‰ at 298K). During the daytime the $\Delta\delta^{15}N_{NOx}$ shifts -30 to -35‰ as the photolysis and $O_3$ isotope effects begin to influence the

https://doi.org/10.5194/gmd-2020-114
Preprint. Discussion started: 22 June 2020

Geoscientific Model Development Discussions
Open Access

$\Delta\delta^{15}N_{NO\text{-}NO2}$. $HNO_3$ $\delta^{15}N$ values during the high $NO_x$ mixing ratio simulation initially follow the $\delta^{15}N$ of $NO_2$ (via $NO_2$ + OH) before approaching 0‰, the defined $NO_x$ source values.

At low $NO_x$ mixing ratios (1.5 ppb, 1/3 NO, 2/3 $NO_2$, Fig. 9c) the $\Delta\delta^{15}N_{NO\text{-}NO2}$ and $HNO_3$ $\delta^{15}N$ is very different from the high $NO_x$ simulation. The nighttime $\Delta\delta^{15}N_{NO\text{-}NO2}$ ranges from -15 to -20‰ and during the daytime it is around +7‰, while the $HNO_3$ $\delta^{15}N$ values hover around zero throughout the simulation. The difference between the $NO_y$ $\delta^{15}N$ values in the high and low $NO_x$ cases can be explained as a competition between the $NO_x$ EIE and the Leighton isotope effect. At high $NO_x$ mixing ratios, the $NO_x$ EIE achieves equilibrium quickly at night ($\Delta\delta^{15}N_{NO\text{-}NO2}$ = -40) because the rate of $NO_x$ isotope exchange (R238) is proportional to its concentration. In contrast, isotope exchange is slow in the low $NO_x$ case and the time scale to reach equilibrium is much longer. Indeed, at the low $NO_x$ mixing ratios the nighttime equilibrium only reaches about 40-50% of completion by 6:30. Afterwards sunlight begins to erase the $NO_x$ EIE effect until around noon when the $\delta^{15}N$ values of NO is mostly due to the Leighton effect and only a small contribution from EIE (about 5%). For intermediate $NO_x$ mixing ratio case (15 ppb, 1/3 NO, 2/3 $NO_2$, Fig. 9b) the diurnal and week-long $NO_y$ $\delta^{15}N$ trends fall somewhere in between the high and low $NO_x$ simulations.

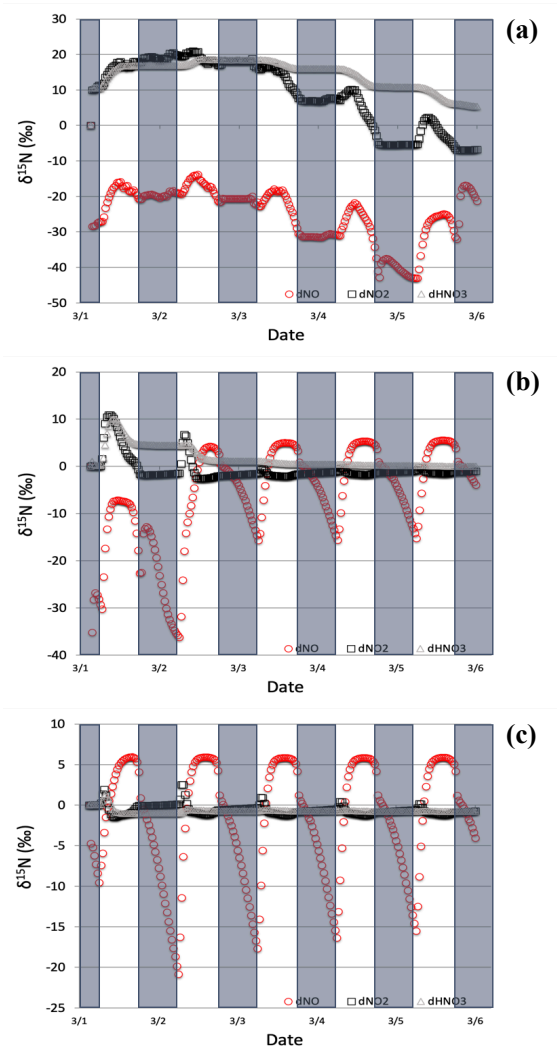


Figure 9. The $\delta^{15}N$ values of $NO_x$ and $HNO_3$ when isotope effects in R1, R48, and R238 are included under high (top, a), medium (middle, b), and low (bottom, c) $NO_x$ scenarios. The 5-day simulation was under the conditions list in Table S3d-f. The $NO_y$ $\delta^{15}N$ values are mainly controlled by $NO_x$ isotope exchange (R238) under high $NO_x$ conditions and Leighton (R1 + R58) under low $NO_x$ conditions.

The changes in $\delta^{15}N$ values of $HNO_3$ during the March 1 simulations at differing $NO_x$ mixing ratios can be explained in terms of $HNO_3$ production pathways. Over the course of day 1 the $\delta^{15}N$ of $HNO_3$ mirrors that of $NO_2$ because $HNO_3$ produced by $NO_2$ + OH (R39), thus the product $HNO_3$ $\delta^{15}N$ values are similar to those in $NO_2$. This varies depending on the $NO_x$ mixing ratio scenario for two reasons. First, as the $NO_x$ mixing ratio gets bigger, the closer the $NO_x$ gets to achieving the EIE and the bigger the split between NO and $NO_2$ $\delta^{15}N$ values (40‰ versus 10‰ for Leighton+$O_3$). Secondly,

https://doi.org/10.5194/gmd-2020-114
Preprint. Discussion started: 22 June 2020



differences in the amount of $NO_x$ result in different $NO/NO_2$ ratios as the simulations progress. For example, under low $NO_x$ mixing ratios the nighttime $NO/NO_2 < .001$, which means the $\delta^{15}N$ value of $NO_2$ will be close to that of total $NO_x$, which will be close to 0‰. At the same time the $\delta^{15}N$ value of NO will be close to the fraction of the EIE achieved, which is about 50% under low $NO_x$ conditions, resulting in a NO $\delta^{15}N$ of about -15‰. These two effects control the $\delta^{15}N$ of $NO_2$ and that in turn controls the $\delta^{15}N$ value of $HNO_3$. In all scenarios the diurnal cycle repeats itself over the subsequent 4 days and a greater fraction of total NO emitted has been turned into $HNO_3$, so that by the end of the 5-day simulation the $HNO_3$ $\delta^{15}N$ values converge towards 0‰, the defined value of $NO_x$ emissions in the simulations.

The modeled $\delta^{15}N$ values of HONO also have a diurnal pattern that can also be traced to diurnal chemistry and isotope mass balance. Similar to the photolysis and photolysis + $O_3$ cases, the HONO $\delta^{15}N$ values mirror the oscillation of the NO $\delta^{15}N$ values (data no shown). This is a result of HONO production by the NO + OH reaction (R38). In contrast, the HONO $\delta^{15}N$ values at night remain nearly constant despite the fact that the $\delta^{15}N$ of NO is changing dramatically. This is because the absence of OH at night halts R38 and thus HONO production ceases and the $\delta^{15}N$ values are simply the same as the residual daytime HONO reservoir. There is a repeated minimum in HONO $\delta^{15}N$ values occurring each morning at 7:00 over the subsequent 4 days. This is a result of the fact that, unlike $HNO_3$, HONO is effectively destroyed by photolysis (R4) and OH (R45). Thus, HONO does not build up in the model over the 5-day simulation, but rather mixing ratio peaks daily (30 ppb) at around 9:00 each day. This is when the HONO production – destruction rate is greatest, and its mixing ratio then deceases to a low of 2 ppt by sunset. Since the nighttime HONO, with $\delta^{15}N \sim +5.5$‰, only contributes about 7% ($f = 0.07$) of the morning HONO spike, it does not greatly impact the control that NO $\delta^{15}N$ has on the HONO $\delta^{15}N$ value. This daily isotope effect should be contrasted with the $HNO_3$ $\delta^{15}N$ trends with time. Initially $HNO_3$ $\delta^{15}N$ values are influenced by $NO_2$ $\delta^{15}N$ variations by $NO_2$-OH-$HNO_3$ coupling, similar to the NO-OH-HONO coupling. But since there is no significant photochemical sink of $HNO_3$, the control on $HNO_3$ $\delta^{15}N$ values by $HNO_3$ accumulation increases with time, so that by day 5 the diurnal changes in $NO_2$ $\delta^{15}N$ have almost no impact on the $HNO_3$ $\delta^{15}N$ values (Fig. 9).

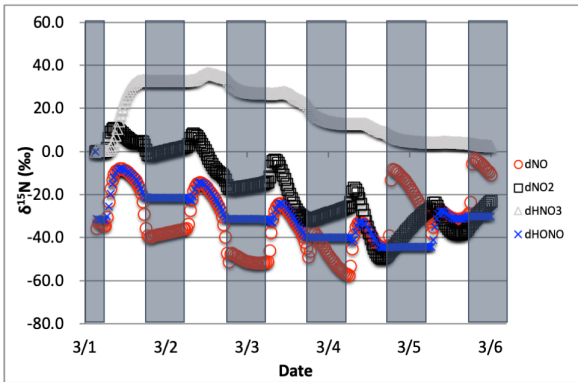


Figure 10. The time evolution of $\delta^{15}N$ values of NO, $NO_2$, $HNO_3$, and HONO caused by isotope effects of Leighton reactions, $NO_x$ isotope exchange, and $NO_2$ + OH reaction, with NO emission, simulation starts from Mar 1. The 5-day simulation was under the conditions list in Table S3c.

### 3.1.4 The $\delta^{15}N$ values of $NO_x$, HONO, and $HNO_3$ due to the combined Leighton cycle, $NO_x$ isotope exchange, and $NO_2$ + OH

The effect of the $NO_2$ + OH reaction has on $\delta^{15}N$ values of $NO_x$ and $HNO_3$ associated was then examined (Table S3c). Since R39 is the last step in $HNO_3$ production, the instantaneous $\delta^{15}N$ $HNO_3 = \delta^{15}N(NO_2) + \varepsilon_{48}$, thus the $\delta^{15}N_{HNO3}$ is initially 40‰ higher than the $NO_2$ (Fig. 10).

https://doi.org/10.5194/gmd-2020-114
Preprint. Discussion started: 22 June 2020



This in turn depletes $^{15}N$ in the residual $NO_2$ leading to more negative $\delta^{15}N$ values in $NO_2$ relative to the Leighton + exchange simulations. These latter two effects are still in play as evident by the diurnal $NO_x$ $\delta^{15}N$ cycling and $\Delta\delta^{15}N_{NO\text{-}NO2}$. As the 5-day simulation progresses, the $HNO_3$ $\delta^{15}N$ value approaches 0‰, approaching the $\delta^{15}N$ of NO emissions, as expected based on isotope mass balance. We point out that this convergence to the source $NO_x$ $\delta^{15}N$ value is much slower in this case than the Leighton and exchanges cases. This highlights the importance of the knowing the correct $\varepsilon_{48}$. If $\varepsilon_{48} \sim 0$ as suggested by Freyer (1993) then daytime the $\delta^{15}N$ $HNO_3 \cong \delta^{15}N$ $NO_2$, demonstrably lower than the $\varepsilon_{48} \sim 40$‰ case. In the end the average daytime $\delta^{15}N$ value of $HNO_3$ for the entire simulation is about 10‰ higher than the $\delta^{15}N$ of the $NO_x$ source (here defined as 0‰).

## 3.2 The $\delta^{15}N$ values of $NO_x$, HONO, and $HNO_3$ due to nighttime chemistry

The role that nighttime chemistry plays in determining the $\delta^{15}N$ values of $NO_x$, HONO, and $HNO_3$ was investigated by iteratively adding relevant fractionation factors to iRACM. The nighttime chemistry effect was assessed by separating the effects of $NO_3$ radical chemistry and $N_2O_5$ heterogeneous hydrolysis. $NO_3$ radical chemistry is only relevant at night because of its short daytime lifetime with respect to photolysis, which keeps its daytime mixing ratios at the sub $ppt_v$ levels [*Platt et al., 1984*]. At night $NO_3$ builds up and produces $HNO_3$ [*Aldener et al., 2006; Finlayson-Pitts and Pitts, 1997; Horowitz et al., 1998*] via reactions with hydrocarbons (R91-97). The magnitude of this isotope effect was tested by adding $NO_3$ the isotope fractionation factors for R91-97 (see methods) and altering VOC emission rates to simulate clean, moderate, and extreme VOC pollution environments. Likewise, $N_2O_5$ only accumulates at night when it begins producing $HNO_3$ on aerosol surfaces [*Chang et al., 2011*]. The magnitude of this isotope effect was tested by adding the $N_2O_5$ EIE (see methods) and adding the first order $N_2O_5$ heterogeneous pathway (see methods) to $i_N$RACM. The first-order rate constant was adjusted to simulate clean, polluted, and extreme pollution environments where aerosol surface area density largely controls the rate constant [*Riemer et al., 2003 Chang et al., 2011*].

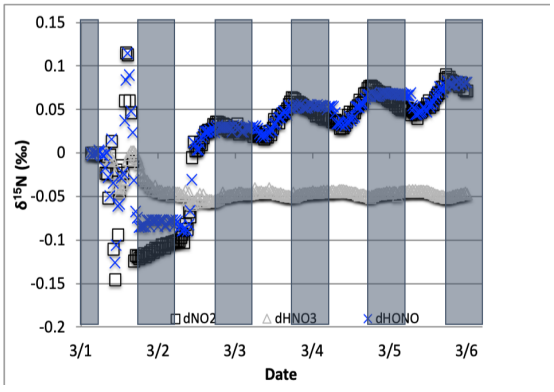


Figure 11. The difference between the $\delta^{15}N$ values of $NO_2$, HONO, and $HNO_3$ when $NO_3$ + VOC → $HNO_3$ reactions are included and excluded (NO was omitted for clarity). The 5-day simulation was under the conditions list in Table S3e. Total VOC mixing ratios during the last day of the March 1 simulation was 550-670 ppb C.

### 3.2.1 The $\delta^{15}N$ values of $NO_x$, HONO, and $HNO_3$ due to $NO_3$ + VOC reactions

The effect on the $\delta^{15}N$ values of $NO_x$, $HNO_3$, HONO associated with the KIE occurring during $NO_3$ + VOC nighttime reactions (R91-R97) were first examined. Four simulations were run that included the isotope effects ($\alpha$ values in Table S6) of the Leighton cycle (R1 and R48), $NO_x$ isotope exchange (R238), $NO_2$ + OH production of $HNO_3$ (R39), and the KIE effects (R91-

https://doi.org/10.5194/gmd-2020-114
Preprint. Discussion started: 22 June 2020



R97), as well as NO emissions. The simulation tested first was the March test case (medium VOC ~360 $ppb_v$). Then, two simulations were run for June 1 (extended sunlight, warm temperatures), one with high initial of VOC concentrations and a high VOC emission rate (2 $ppb_v$ $h^{-1}$) and one with low emission rate of VOCs (0.4 $ppb_v$ $h^{-1}$). The same two initial conditions were used in the Jan. 1 test case to assess if the extended night time and cold temperatures significantly affected the $NO_x$ of $HNO_3$ $\delta^{15}N$ values produced by $NO_3$ radicals. The impact of $NO_3$ reactions on $NO_y$ $\delta^{15}N$ values was determined by subtracting these simulated $\delta^{15}N$ values from those same simulations when only the Leighton cycle, exchange and OH + $NO_2$ reaction was considered (Section 3.1).

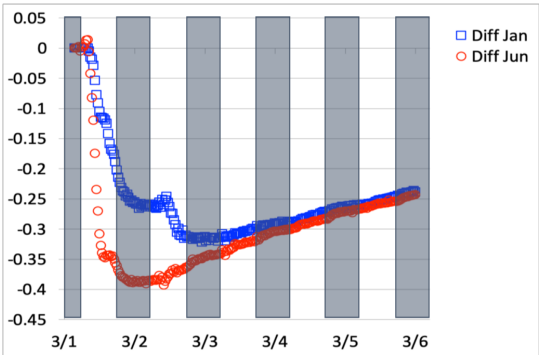


Figure 12. The difference in $\delta^{15}N(HNO_3)$ values when $NO_3$ + VOC → $HNO_3$ reactions are included and excluded, for Mar 1 simulation, relative to Jun 1 simulation (☐) and Jan 1 simulation (o). The 5-day simulation was under the conditions list in Table S3e.

The $NO_3$ + VOC KIE induced a minor diurnal pattern on the $\delta^{15}N$ values of $NO_x$, and HONO, and a trend for $HNO_3$ for the March test case, but the size of the effect was relatively small (e.g., < 0.4‰; Fig. 11). At the start of the simulation (3 am) there is no $HNO_3$, therefore the initial $HNO_3$ is produced via OH production of $HNO_3$ (R39),

$\delta^{15}N$ values of $HNO_3$ decreased from 0.35 to 0.2‰ during the night. The pattern is because of increasing the importance of R91-R97 in $HNO_3$ production at night. The smallness of the effect is because $\alpha$ values are all relatively small, the average $\delta$ for the $NO_3$ + VOC is about -4‰, and the relatively small amount of $HNO_3$ produced via these pathways (around 2.6 % of 24-hour $HNO_3$). The first source of the $HNO_3$ in the simulation (3 to 6 am) is the $NO_3$ + VOC reactions and results in a slight negative $\delta^{15}N$ in $HNO_3$ value (-0.01‰). This leaves the residual $NO_3^-$ $^{15}N$ enriched that is then photolyzed into $NO_2$ at sunrise and used $NO_2$ + OH → $HNO_3$ production resulting in slight positive $\delta^{15}N$ values (+0.35‰) (Fig. 11). The range of the diurnal $HNO_3$ $\delta^{15}N$ oscillation dampens as the fraction of emitted NO that has been converted to $HNO_3$ has increased over time. The diurnal and weekly change in $\delta^{15}N$ of $HNO_3$ changes did not significantly change during the winter and summer simulations (Fig. 12) run with and without the KIE for R91-R97 show negligible differences, similar to those in Fig. 11. In conclusion, although there is some $\delta^{15}N$ effect associated with $NO_3$ + VOC chemistry, it is much smaller than the effects associated with the

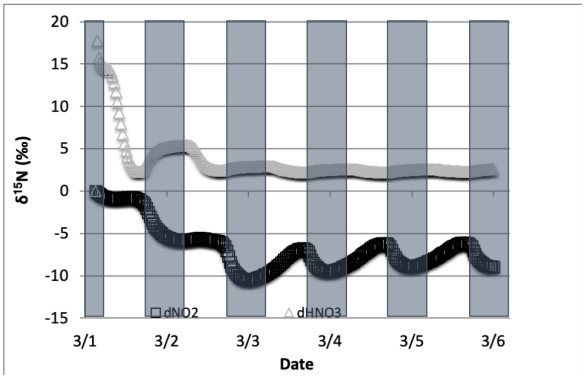


Figure 13. The difference in $\delta^{15}N$ values of $NO_2$ and $HNO_3$ when the isotopic effect during $N_2O_5$ heterogeneous reactions (R53-54, R239) is included ($\alpha_{N2O5}$ =1.029) and when it is excluded ($\alpha_{N2O5}$ = 1.0). The 5-day simulation was under the conditions list in Table S3e.

https://doi.org/10.5194/gmd-2020-114
Preprint. Discussion started: 22 June 2020



Leighton cycle, $NO_2$ + OH, and $NO_x$ equilibrium.

### 3.2.2 The $\delta^{15}N$ values of $NO_x$, HONO, and $HNO_3$ due to $N_2O_5$ reactions

The effect on the $\delta^{15}N$ values of $NO_x$, $HNO_3$, HONO associated with the EIE of $N_2O_5$ heterogeneous hydrolysis was also tested. March 1 simulations with N emissions and $k_{N2O5}$ = 0.1 $s^{-1}$ were run that included the isotope effects of the Leighton cycle (R1 and R48), $NO_x$ isotope exchange (R238), OH production of $HNO_3$ (R39), and the $N_2O_5$ EIE (R53-54) KIE (R239) (Table S7), as well as NO emissions. These simulations were compared to an identical simulation but where the $\alpha_{N2O5}$ was set equal to 1.0. This ensured that the $NO_y$ chemistry was not altered when comparing the two simulations (i.e., $\alpha_{N2O5}$ = 1.029 vs. $\alpha_{N2O5}$ = 1.0). The effect of $N_2O_5$ chemistry on the $\delta^{15}N$ values of $NO_2$ and $HNO_3$ was investigated. Similar to the March 1 $NO_3$ + VOC tests, simulations with R1, R39, R48, R238, and R239 isotope effects active were run and then compared to simulations with the same conditions but with R239 turned off. In addition, March simulations were run using three different $k_{N2O5}$ values (.01, 0.1 and 1) and compared to each other in order to test the range of $NO_2$ and $HNO_3$ $\delta^{15}N$ values that could be generated solely by heterogeneous $N_2O_5$ hydrolysis.

The average daily $\delta^{15}N$ values of $HNO_3$ exhibit some diurnal oscillations that roughly reach a steady state average value after simulation day 2. At that point $HNO_3$ has a $\delta^{15}N$ = +2.5‰ relative to the $\alpha_{N2O5}$ = 1.0 simulation. In contrast the $NO_2$ $\delta^{15}N$ values oscillate diurnally by about +/- 2‰ around an average daily difference of about -8‰. This change is due to the R53-54 equilibrium, which predicts $^{15}N$ enrichment in $N_2O_5$ (and thus $HNO_3$) and depletion in $NO_3$ and $NO_2$. The $N_2O_5$ produces $HNO_3$ with the highest $\delta^{15}N$ difference (~ +29‰) during the first simulation morning. This is because all of the initial $HNO_3$ is produced by $N_2O_5$ due to the 3 am simulation start time. The roughly steady state $HNO_3$ $\delta^{15}N$ value of +2.5‰ is a consequence of the fact that when $\alpha_{N2O5}$ = 1.0 $HNO_3$ is being produced by $N_2O_5$ at 0‰ and when $\alpha_{N2O5}$ =1.029 it is being produced at +29‰. The ratio of this simulated +2.5‰ value and $N_2O_5$ enrichment factor of +29‰ yields 0.086, the fraction of $HNO_3$ produced by $N_2O_5$. This is similar to the fraction of $HNO_3$ produced in simulations when the $N_2O_5$ reaction was active and where it is inactive, which yielded a fraction of 0.064. The difference in these fractions is because deactivating $N_2O_5$ chemistry changes overall $NO_y$ chemistry and $HNO_3$ production *[Dentener and Crutzen, 1990]*.

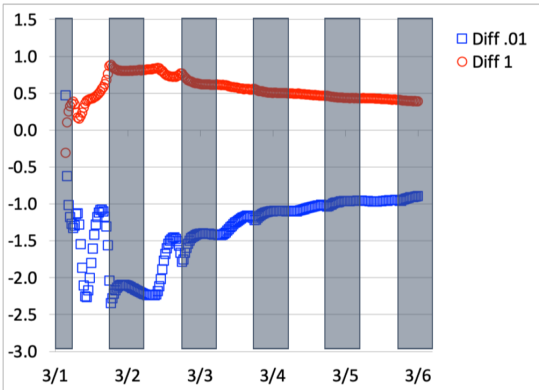


Figure 14. The difference in $\delta^{15}N(HNO_3)$ values when the isotopic effect during $N_2O_5$ heterogeneous reactions is included and when it is excluded, for the simulation of $k_{N2O5}$ = 0.1, relative to 0.01 (□) and 1.0 (o). The 5-day simulation was under the conditions list in Table S3e.

The effect of $N_2O_5$ chemistry on the $\delta^{15}N$ values of $NO_2$ is more dynamic than $HNO_3$ (Fig. 13). This is mainly due to the fact that $HNO_3$ is continually building up over time and thus its $\delta^{15}N$ is less susceptible to change by small additions. The oscillation in the $NO_2$ $\delta^{15}N$ value

https://doi.org/10.5194/gmd-2020-114
Preprint. Discussion started: 22 June 2020



becomes more negative at night, which corresponds to the increase in the $HNO_3$ $\delta^{15}N$ values. This is a reflection of $^{15}N$ preferentially incorporating into $N_2O_5$ resulting in $NO_2$ depleted in $^{15}N$. Similar oscillations are found in NO and HONO (data not shown) as they are connected to $NO_2$ build-up and decay diurnally. This suggests that night-time partitioning of $NO_y$ will have a small but measurable influence on daytime $NO_y$ $\delta^{15}N$ values. The effect of using different $k_{N2O5}$ values had a small but measurable effect on the $NO_2$ and $HNO_3$ $\delta^{15}N$ values. Simulations that used a $k_{N2O5}$ = 1.0 resulted in $HNO_3$ $\delta^{15}N$ values that were about 2‰ lower than those run at $k_{N2O5}$ = 0.01 and 1‰ heavier than when $k_{N2O5}$ = 1.0. This makes sense because the mean EIE for $N_2O_5$ (29‰) is lower than that for $NO_2$ + OH (40‰), therefore as $N_2O_5$ produces more $HNO_3$ its $\delta^{15}N$ value would decrease with respect to that of daytime $HNO_3$ production. Thus, the model predicts lower $HNO_3$ $\delta^{15}N$ values in cold, dark polluted regions (relative to the tropics where) where $N_2O_5$ heterogeneous hydrolysis may be the main $HNO_3$ production pathway *[Dentener and Crutzen, 1990]*.

## 3.3 Case studies

The completed $i_N$RACM was tested using different simulation conditions that had various initial trace gas concentrations and emission rates. These test cases were labeled urban, rural, forest, and marine due to their initial conditions that were designed to mimic those environments. Initially, $i_N$RACM simulations were run using the 18 test cases without emission (9 for urban condition, 9 for rural condition), and 2 test cases with emission (1 for polluted atmosphere, 1 for clean atmosphere) provided in Stockwell *(1997)*. However, we found that trace gas concentrations in these simulations do not agree with atmospheric observations (See SI) when simulations were run for several days *[Altshuller, 1989; Baugues, 1986; Greenberg & Zimmerman, 1984; Logan, 1989; National Research Council, 1992; Torres & Buchan, 1988; Zimmerman et al., 1988]*. Thus, instead of replicating Stockwell's cases (See SI), we set up four conditions that mimic urban, rural, forest, and marine, with the initial concentrations based on various measurements from previous studies. The emission rates of NO and total VOCs were tuned until the simulation results satisfied with the following features: a). The concentration of $NO_x$ changes diurnally and stabilized through time; b). The concentration of $O_3$ changes diurnally and stabilized through time; c). VOCs are slowly consumed during nighttime (Fig. S2-5). The molar fraction of each VOC species with respect to the total VOC emission rate was obtained from Stockwell's *(1997)* emission cases. It is noted that the conditions chosen for urban, rural, forest, and marine may not be representative of all of these environments in different countries or regions (i.e all urban environments are not the same) but were devised to bracket extremes of trace gases for most tropospheric conditions (we have ignored any polar environment simulations due to isotope effects occurring during snow pack photolysis).

### 3.3.1 The initial concentrations and emission rates under the urban conditions

The simulations under the urban conditions were designed to simulate highly polluted urban environments such as current Asia megacities and early 1980's US cities. The initial concentration of $NO_x$ (Table S8) was set to 180 ppb, based on 90$^{th}$ percentile of polluted US cities (Cincinnati, OH, Fort Worth, TX, Memphis, TN, Miami, FL, Cleveland, OH) during summers of 1984 and 1985 *[Baugues, 1986]*, slightly lower than the maximum $NO_x$ concentration (> 200 ppb) at Shenyang, China from Aug 20 to Sept 16, 2017 *[Ma et al., 2018]*.

https://doi.org/10.5194/gmd-2020-114
Preprint. Discussion started: 22 June 2020



For urban conditions, $NO/NO_x$ ratio was set to 0.5 and $NO_x/NO_y$ ratio was set to 0.9, and we assumed the concentrations of $HNO_3$ and PAN are equal since they are minimal $NO_y$ compounds in this case. The initial carbon (C) concentration of total VOC was set to 1000 ppb C, based on the weighted average of the measurements among 30 sites during the summers of 1984 and 1985 *[Baugues, 1986]*. Baugues *(1986)* also provided the carbon fraction of toluene, xylene, HCHO, acetaldehyde, ethene, alkene other than ethene, and total alkane with respect to total VOC in ppb C. Thus, the initial concentration of toluene, xylene, HCHO, acetaldehyde, ethene was based on their carbon fraction provided by Baugues *(1986)*. The initial concentration of each alkane and alkene species was based on the carbon fraction of their groups, provided by Stockwell et al. *(1997)*. Thus, the initial concentration of total VOC was set to 252 ppb, which matches well with the recent year measurement at Shenyang, a typical urban area of Northeast China *[Ma et al., 2018]*. To stabilize the concentration of $NO_x$, the emission rates of NO and total VOCs were set to 9.36 ppb $h^{-1}$ and 7.80 ppb $h^{-1}$, respectively. The initial concentration of $O_3$ at 300 ppb, which is closed to the average among five most polluted sites from the measurement among Northeastern United States in the 1970's *[Cleveland et al., 1977]*, and the maximum value (286 ppb) measured within three main megalopolises in China (Jinjinji, Yangtze River Delta, and Pearl River Delta) from 1997 to 2016 *[Wang et al., 2017]*. During the simulations, the $O_3$ concentration stabilized, with summertime maximum hourly concentration around 200 ppb, which agree well with previous studies (National Research Council, 1992).

3.3.2 The initial concentrations and emission rates under the rural conditions

The simulations under the rural conditions were designed to simulate moderately polluted environments upwind of such current Asia megacities and early 1980's US cities. The initial concentration of $NO_x$ was set to 7 ppb (Table S8), based on the average of 120 samples collected aloft upwind of six US cities (Dallas-Fort Worth, TX, Tulsa, OK, Birmingham, AL, Atlanta, GA, Philadelphia, PA, New York, NY) during summers of 1985 and 1986 *[Altshuller, 1989]*. The 7 ppb $NO_x$ also matches well with the value measured in Baltimore/Washington airshed in 2011 *[He et al., 2013]*. For rural condition, $NO_x/NO_y$ ratio was set to 0.44, based on the average ratio among previous studies *[Carroll et al., 1992; Fahey et al., 1986; National Research Council, 1992; Parrish et al., 1986; Williams et al., 1987]*, $NO/NO_x$ ratio was set to 0.7. According to Logan *(1989)*, the ratio between $NO_x$ and PAN has a median value of around 2.5. Thus, the initial concentrations of NO, $NO_2$, $HNO_3$, and PAN are 4.9 ppb, 2.1 ppb, 6 ppb, and 3 ppb, respectively (Table S8). The initial concentrations of each VOC species were based on the weighted average of the measurements, upwind of the six US cities. The 8.3 ppb initial concentration of total OC matches well with the recent year measurement in the rural area of Midwest, US *[Sjostedt et al., 2011]*. The initial concentration of $O_3$ was set to 50 ppb, based on the average summertime $O_3$ concentration among rural areas *[Cooper et al., 2012, Janach, 1989; Logan, 1989]*. To stabilize the concentration of $NO_x$ and $O_3$, the emission rates of NO and total VOCs were set to 0.24 ppb $h^{-1}$and 0.59 ppb $h^{-1}$, respectively.

3.3.3 The initial concentrations and emission rates under the forest conditions

The simulations under the forest conditions were designed to simulate low polluted environments (Table S8), with high emissions of biogenic VOCs such as isoprene. The initial concentration of $NO_x$ was set to 0.06 ppb, which is the minimum concentration at the central basin of Amazon tropical forest *[Torres and Buchan, 1988]*. Typically, at the remote sites (forest and marine condition), the ratio of $NO_x/NO_y$ is between 0.1 and 0.2, $HNO_3/NO_x$ is less than 5,

https://doi.org/10.5194/gmd-2020-114
Preprint. Discussion started: 22 June 2020



and PAN/$NO_x$ is less than 1 *[Carroll et al., 1992]*. To satisfy all three conditions, the initial concentration of $HNO_3$ and PAN were set to 0.29 ppb and 0.05 ppb, respectively. NO/$NO_x$ ratio was set to 0.9. Thus, NO and $NO_2$ equal to 0.054 ppb and 0.006 ppb, respectively. The initial concentrations of each VOC species were based on the median concentration of 81 samples in Amazon *[Zimmerman et al., 1988]*. The 6.7 ppb initial concentration of total VOC matches well with the recent year measurement in Amazon *[Fuentes et al., 2016]*. The initial concentration of $O_3$ was set to 10 ppb, which is closed to the average hourly concentration during the summertime in Amazonia *[Fuentes et al., 2016, Kirchhoff, 1988]*. To stabilize the concentration of $NO_x$ and $O_3$, the emission rates of NO and total VOCs were set to 9.4 ppt $h^{-1}$ and 0.35 ppb $h^{-1}$, respectively.

3.3.4 The initial concentrations and emission rates under the marine conditions

The simulations under the marine conditions were designed to simulate remote, clean oceanic environments. The initial concentration of $NO_x$ was set to 0.03 ppb (Table S8), which is the medium value of 28,974 data points, measured simultaneously at Mauna Loa, Hawaii, from May 1 to June 4, 1988 *[Carroll et al., 1992]*, as well as at Cape Norman, Canada, northern Atlantic coastal site, from February to April, 1996 *[Yang et al., 2004]*. Typically, at the remote sites (forest and marine condition), the ratio of $NO_x/NO_y$ is between 0.1 and 0.2, $HNO_3/NO_x$ is less than 5, and PAN/$NO_x$ is less than 1 *[Carroll et al., 1992]*. To satisfy all three conditions, the initial concentration of $HNO_3$ and PAN were set to 0.145 ppb and 0.025 ppb, respectively. NO/$NO_x$ ratio was set to 0.9. Thus, NO and $NO_2$ equal to 0.027 ppb and 0.003 ppb, respectively. The initial concentrations of each VOC species were based on the median values between the sample collected by two cruises over the tropical Pacific Ocean, during December 1982, and July 1982, respectively *[Greenberg and Zimmerman, 1984]*. The 5.4 ppb initial concentration of total VOC matches well with the recent year measurement over the western North Pacific and eastern Indian Ocean *[Saito et al., 2000]*. The initial concentration of $O_3$ was set to 10 ppb, which the average summertime concentration among maritime sites in both the north and south hemispheres *[Janach, 1989]*. To stabilize the concentration of $NO_x$ and $O_3$, the emission rates of NO and total VOCs were set to 12.48 ppt $h^{-1}$ and 0.234 ppb $h^{-1}$, respectively

3.3.5 The simulated $\delta^{15}N$ value under the urban conditions

The simulated $\delta^{15}N$ values of $NO_x$ under the urban conditions have extreme diurnal oscillations and almost no weekly trend. The most striking feature is the extreme diurnal oscillations in NO and $NO_2$ $\delta^{15}N$ values. During the early nighttime (1/2, 6/2) the NO and $NO_2$ $\delta^{15}N$ values are similar (~ -5‰, $\Delta\delta^{15}N_{NO\text{-}NO2}$ =+20 ‰), but they diverge over about a 6 hour period until reaching a maximum $\Delta\delta^{15}N_{NO\text{-}NO2}$ = -35 +/- 5%. At this point, the NO $\delta^{15}N$ value has reached its minimum values of -38‰ (Jan 1) and -36‰ (June 1), which corresponds to minimums in the $f_{NO}$ and NO mixing ratio (SI Fig x). Meanwhile, the $\delta^{15}N$ values of $NO_2$ approach 0‰ as its mixing ratio and $f_{NO2}$ have reached maximums. This indicates that the $NO_x$ isotopic exchange ($\varepsilon_{NO/NO2}$ = -35‰ at 298K) is dominating the $NO_x$ isotopic effects during the night and that under these conditions it requires about 6 hours for $NO_x$ to achieve full isotopic equilibrium.

https://doi.org/10.5194/gmd-2020-114
Preprint. Discussion started: 22 June 2020



In contrast, during the daytime, the NO and $NO_2$ $\delta^{15}N$ values are influenced by photolysis and Leighton cycle isotope effects. In the morning, the split between NO and $NO_2$ $\delta^{15}N$ values is eliminated as $NO_2$ is photolyzed. This is, in large part, a simple isotope mass balance effect because isotopically heavy (nighttime) $NO_2$ is now producing isotopically heavy NO causing the NO $\delta^{15}N$ values to increase, closely following the $f_{NO}$ (SI Fig. x). The $NO_2$ PHIFE ($\varepsilon_{R1a}$ = 2.3‰ at 45 degree of solar zenith angle), however, must also be in play otherwise $NO_2$ $\delta^{15}N$ values would not decrease in the early morning. The $NO_2$ PHIFE, however, cannot account for the roughly 20‰ decrease in the $NO_2$ $\delta^{15}N$ values over the course of the mid-morning. This extra decrease is the result of $NO_2$ + OH ($\varepsilon_{39a}$ = 40‰) which depletes the residual $NO_2$ $\delta^{15}N$ values and results in an $HNO_3$ $\delta^{15}N$ increase, which maximizes around noon each day (Fig. 15). This $\varepsilon_{39a}$ effect reduces in importance in the late afternoon as OH mixing ratios decrease and the rate of R39 decreases to zero. The $NO_x$ $\delta^{15}N$ equivalence point ($NO_2$ $\delta^{15}N$ ≈ NO $\delta^{15}N$) occurs around noon in June and early evening in January, and corresponds to the $NO_2$ $\delta^{15}N$ minimum values of ~ -15 to -20 ‰. This highlights the fact that actinic flux plays a key role in controlling the rate of $NO_x$ $\delta^{15}N$ oscillation rates. The combined Leighton cycle isotope effects eventually push NO $\delta^{15}N$ values above the $NO_2$ values, which occurs sooner in the June simulation than the Jan. because of higher $NO_x$ Leighton cycle turnovers caused by higher photolysis rates and $O_3$ mixing ratios (maximums 316 $ppb_v$ versus 236 $ppb_v$). Thus, unlike nighttime, when $NO_x$ isotope exchange controls $NO_x$ $\delta^{15}N$ values, photolysis and Leighton cycle and R39 isotope effects control daytime $NO_x$ $\delta^{15}N$ values that in turn control HONO and $HNO_3$ $\delta^{15}N$ values.

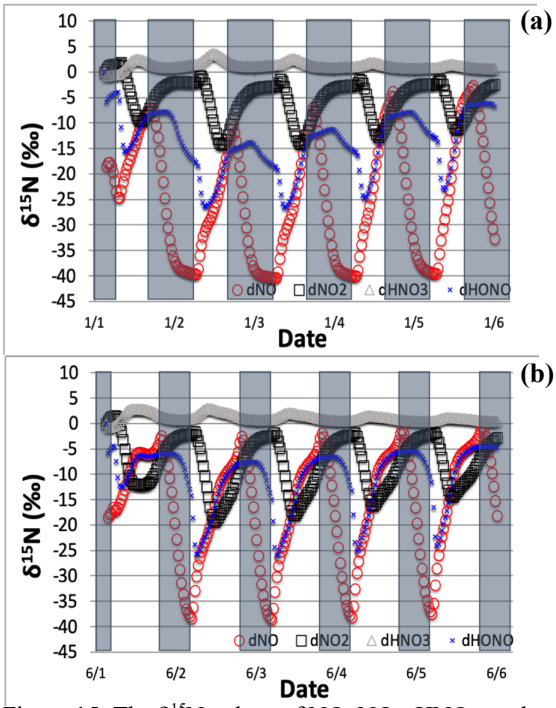

Figure 15. The $\delta^{15}N$ values of NO, $NO_2$, $HNO_3$, and HONO for urban condition for Jan 1 (top, a) and Jun 1 (bottom, b) simulation. The 5-day simulation was under the conditions list in Table S8.

The $\delta^{15}N$ values of HONO mimic the $\delta^{15}N$ values of NO during the daytime because of the production by the NO + OH reaction (R38). This mimicking is most obvious in the non-urban simulations where daytime HONO and NO $\delta^{15}N$ values are the same during the day, afterward, the HONO $\delta^{15}N$ decouples and remains constant during the night when OH is absent (Fig. 16-18). Interestingly, unlike the non-urban simulations, the urban nighttime HONO $\delta^{15}N$ does not remain constant. There is a slight increase in HONO $\delta^{15}N$ values earlier during the late evening, then the $\delta^{15}N$ values of HONO decrease dramatically to approach the $\delta^{15}N$ values of NO after midnight (Fig. 15). Since no HONO isotope effects included in the current $i_N$RACM, this nighttime effect was traced to nighttime OH production under high pollution conditions. During the daytime, OH

https://doi.org/10.5194/gmd-2020-114
Preprint. Discussion started: 22 June 2020



is produced by the reaction of water vapor with $O^1D$, which arises from ozone photolysis. In contrast, during the night, due to the absence of photolysis, the production of OH is usually assumed to be zero. However, under high VOCs, the $i_N$RACM model simulates OH production through a 2-step process. First, production of $HO_2$ by VOC + $NO_3$ reactions (R91, R93, R96) followed by the production of OH by $HO_2$ + $NO_x$ reactions (R41-R44). Under the urban condition, the relatively high VOC concentration promotes the production of $HO_2$ by VOC + $NO_3$, and relatively high ozone concentration leads to higher $NO_2$ and $NO_3$ concentration during the early evening, resulting in the production of OH by $HO_2$ + $NO_x$ reactions (R41-R44). Because of the production of HONO by the NO + OH reaction (R38), the $\delta^{15}N$ values of HONO starts approaching the nighttime $\delta^{15}N$ values of NO, when the concentration of OH becomes sufficiently high. This effect can be seen in the changing OH mixing ratios during the urban night (SI Fig. X).

The daily $HNO_3$ $\delta^{15}N$ values reach a daily maximum around noon each simulation day and trend toward 0‰ at night and by the end of the week. The initial $HNO_3$ $\delta^{15}N$ values are near 0‰ because the initial $HNO_3$ is set to 0‰ (Table S8). Afterward, the daily $HNO_3$ $\delta^{15}N$ values reach midday maximums, ~4‰ for Jan 1 and 3‰ for June 1 simulations, which corresponds to the maximums in OH concentration and $HNO_3$ produced by the R38 pathway. The $\delta^{15}N$ values of $HNO_3$ decrease during the late afternoons and nighttime, as the $\delta^{15}N$ of the reacting $NO_2$ decreases and as isotope effects of $NO_3$ +VOCs and $N_2O_5$ become effective. During this 5-day simulation, the $HNO_3$ concentrations gradually reach quasi-equilibrium, as an increasing amount of $NO_x$ is converted into $HNO_3$. As a result, the small diurnal cycle in $HNO_3$ $\delta^{15}N$ values becomes less obvious going from simulation day 1 to day 5 where it approaches 0‰, the default $\delta^{15}N$ of $NO_x$ emissions, which obeys the N isotope mass balance. In June 1 simulation, the rate and duration of ozone photolysis is higher, thus more $O^3P$ is produced, comparing to Jan 1 simulation. As a result, the concentration of $NO_3$ during the late afternoon is higher, causing the isotope effect of $NO_3$ +VOCs reaction being stronger. Therefore, the $\delta^{15}N$ values of $HNO_3$ in June 1 simulation reaches the maximum value and approaches to 0‰ faster than in Jan 1 simulation.

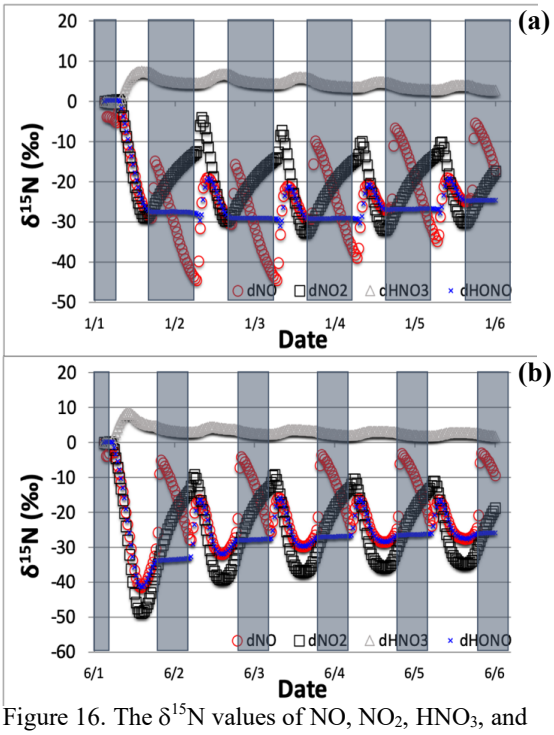

Figure 16. The $\delta^{15}N$ values of NO, $NO_2$, $HNO_3$, and HONO for rural condition for Jan 1 (top, a) and Jun 1 (bottom, b) simulation. The 5-day simulation was under the conditions list in Table S8.

3.3.6 The simulated $\delta^{15}N$ value under the rural conditions

The simulated $\delta^{15}N$ values of $NO_x$ under the rural conditions shows similar, yet strikingly different, diurnal and weekly trends compared to urban simulation. This difference is mainly due to the longer $NO_x$ isotope equilibrium timescale under lower $NO_x$ conditions. The $\Delta\delta^{15}N_{NO\text{-}NO2}$ decreases

https://doi.org/10.5194/gmd-2020-114
Preprint. Discussion started: 22 June 2020



during the nighttime and reaches the -15.3‰ (June 1) just before sunrise indicating that $NO_x$ isotopic exchange ($\varepsilon_{NO/NO2}$ = -40‰ at 298K) is not reaching full equilibration during the night.

Similar to urban simulation, $\Delta\delta^{15}N_{NO\text{-}NO2}$ in Jan 1 simulation is lower than in June 1 simulation, caused by more remaining amount of $NO_x$ after weaker $NO_2$ photolysis during the daytime. The $NO_x$ isotopic exchange is weaker, comparing to the urban simulation, due to the lower $NO_x$ concentrations. Therefore, the decrease of $\Delta\delta^{15}N_{NO\text{-}NO2}$ during the nighttime is less obvious than urban simulation. The $\Delta\delta^{15}N_{NO\text{-}NO2}$ gradually increases during the daytime, as the photolysis ($\varepsilon_{R1a}$ = 2.3‰ at 45 SZA), $O_3$ + NO ($\varepsilon_{48a}$ = -6.7‰), and $NO_2$ + OH ($\varepsilon_{39a}$ = 40‰) isotope effects become effective. The maximum daytime $\Delta\delta^{15}N_{NO\text{-}NO2}$ reaches at sunset, showing 5.5‰ for Jan 1 simulation and 8.5‰ for June 1 simulation. The $\Delta\delta^{15}N_{NO\text{-}NO2}$ increases by 37.6‰ and 23.8‰ during the daytime for Jan 1 and June 1 simulation, respectively, which indicates the dominance of $NO_2$ + OH reaction (R39). Compared to urban simulation, change of $\Delta\delta^{15}N_{NO\text{-}NO2}$ during the daytime is smaller, caused by weaker isotope effect from $O_3$ + NO (R48) reaction, because of lower ozone concentration. The change of $\Delta\delta^{15}N_{NO\text{-}NO2}$ during the daytime for June 1 simulation is larger than that for Jan 1 simulation, due to the higher rate and longer duration of $NO_2$ photolysis.

Similar to the urban simulation, the $\delta^{15}N$ values of HONO mimics the $\delta^{15}N$ values of NO during the daytime because of the production by the NO + OH reaction (R38), of which the fractionation factor ($\alpha$) is zero. Unlike urban simulation, however, the $\delta^{15}N$ values of HONO remain constant at night, since the concentration of $HO_x$ (OH + $HO_2$) is not enough to produce HONO, due to the relatively low VOC (3.3% of urban value) and ozone (16.7% of urban value) concentration. A key caveat about the $\delta^{15}N$ values of HONO is that we have excluded any KIE associated with the NO + OH reaction because it has not been measured or calculated. Since this is the termination reaction, any isotope effect in this reaction would have a large influence on HONO $\delta^{15}N$ values. In the forest and ocean environment simulations, the $\delta^{15}N$ values of HONO also mimic the $\delta^{15}N$ values of daytime NO so they will not be discussed in the subsequent sections of this paper.

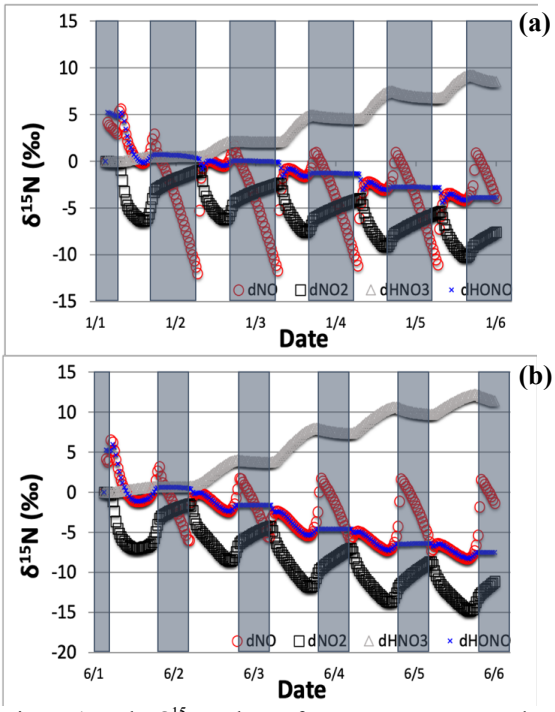

Figure 17. The $\delta^{15}N$ values of NO, $NO_2$, $HNO_3$, and HONO for forest condition for Jan 1 (top, a) and June 1 (bottom, b) simulation. The 5-day simulation was under the conditions list in Table S8.

The $\delta^{15}N$ values of $HNO_3$ increases during the mornings and reaches the maximum of 7.5‰ for Jan 1 simulation and 8.4‰ for June 1 simulation, as the isotope effects of $NO_2$ + OH ($\varepsilon_{39a}$ = 40‰) greater than $NO_3$ +VOCs ($\Sigma\varepsilon_{91a\sim\varepsilon97a}$ = -27.8‰). The maximum $\delta^{15}N$ value of $HNO_3$ is higher than that in urban

https://doi.org/10.5194/gmd-2020-114
Preprint. Discussion started: 22 June 2020



simulation, as the lower VOC concentration weakens the $NO_3$ +VOCs reactions. The $\delta^{15}N$ values of $HNO_3$ decreases during the late afternoons and nighttime, as the isotope effects of $NO_3$ +VOCs are effective. The same as urban simulation, the diurnal trend of $\delta^{15}N(HNO_3)$ becomes less obvious from simulation day 1 to day 5 and approaches 0‰ at the end of the simulation, as an increasing amount of $NO_x$ being converted into $HNO_3$. Again, the $\delta^{15}N$ values of $HNO_3$ in June 1 simulation approaches to 0‰ faster than in Jan 1 simulation, due to more $O(^3P)$ from stronger $O_3$ photolysis.

3.3.7 The simulated $\delta^{15}N$ value under the forest conditions

The simulation of $\delta^{15}N$ values of $NO_x$ under the forest conditions shows similar, yet significantly different diurnal and weekly trend, comparing to urban and rural simulation. There are obvious differences between the daily oscillations in $NO_2$ $\delta^{15}N$ values in the forest relative to urban simulations. In the cleaner atmosphere, $NO_2$ $\delta^{15}N$ values only change daily by only about 5‰, whereas they oscillate by 30 to 40‰ in the urban case. Likewise, daily oscillations in NO $\delta^{15}N$ values are weaker in the forest conditions (5-10‰) than in the urban and suburban conditions (30-40‰). This results in a decrease in the $\Delta\delta^{15}N_{NO\text{-}NO2}$ during the nighttime, reaching minimum values of -11.0‰ (Jan 1) and -4.5‰ (June 1) compared to roughly -40‰ in the urban case. This shows that under low $NO_x$ conditions the $NO_x$ isotopic exchange cannot occur fast enough to reach its full effect. This effect is more pronounced in June, due to the short night, relative to the January simulations that have about 14 hours of darkness at this latitude. This is similar to urban and rural simulations, where $\Delta\delta^{15}N_{NO\text{-}NO2}$ in Jan 1 simulation is lower than in June 1 simulation, because of reduced $NO_2$ photolysis hours. The decrease of $\Delta\delta^{15}N_{NO\text{-}NO2}$ during the nighttime in the forest conditions is less obvious than urban and rural simulation. The $\Delta\delta^{15}N_{NO\text{-}NO2}$ gradually increases during the daytime, as the photolysis ($\varepsilon_{R1a}$ = 4.2‰), $O_3$ + NO ($\varepsilon_{48a}$ = -6.7‰), and $NO_2$ + OH ($\varepsilon_{39a}$ = 40‰) isotope effects become effective. This results in daytime NO $\delta^{15}N$ values that are less negative than those in $NO_2$, opposite of the urban case where $NO_2$ $\delta^{15}N$ values are either higher or equal to NO. As a consequence, the daytime $\Delta\delta^{15}N_{NO\text{-}NO2}$ values are positive (as opposed to negative in the urban case) and reach a maximum at sunset (6.5‰ for Jan 1, 7.1‰ for June 1). The $\Delta\delta^{15}N_{NO\text{-}NO2}$ increases by 17.5‰ and 13.3‰ during the daytime for Jan 1 and June 1 simulation, respectively, which indicates the dominance of $NO_2$ + OH reaction (R39). The change of $\Delta\delta^{15}N_{NO\text{-}NO2}$ during the daytime is smaller than both urban and rural simulation, due to lower ozone concentration. The change of $\Delta\delta^{15}N_{NO\text{-}NO2}$ during the daytime for June 1 simulation is larger than that for Jan 1 simulation, due to the higher rate and longer duration of $NO_2$ photolysis.

The most striking difference between the "clean" and "polluted" simulations is the separation of $HNO_3$ $\delta^{15}N$ values from the initial (emission) $NO_x$ $\delta^{15}N$ value (defined as 0‰). The $\delta^{15}N$ values of $HNO_3$ increases daily by about 1-4‰ due to the isotope effects of $NO_2$ + OH ($\varepsilon_{39a}$ = 40‰) but are constant or slightly decrease throughout the night due to $NO_3$ +VOCs reactions under these conditions. This leads to a stepwise increase in $HNO_3$ $\delta^{15}N$ values that reach maximums of about +10‰ by the end of the 5-day simulation. This is in contrast to the urban and suburban simulations where $HNO_3$ $\delta^{15}N$ values reach minimums (~ 0‰) at the end of the simulation. This is an isotope mass balance effect driven by how N is partitioned into $NO_y$ under different conditions. Under high $NO_x$ and VOC conditions (urban, rural) over 90% of emitted $NO_x$ has portioned into $HNO_3$ by the end of the 5-day simulation, thus the $HNO_3$ $\delta^{15}N$ value approaches that of the $NO_x$ emissions. In contrast, under low $NO_x$ and VOC conditions (forest,

https://doi.org/10.5194/gmd-2020-114
Preprint. Discussion started: 22 June 2020



ocean) only about 33% of emitted $NO_x$ has portioned into $HNO_3$, with the bulk of remainder as $NO_x$ (21%) and organic nitrate (42%) and PAN (4%). In this case, the isotope effects incorporated into the reactions that are responsible for this partitioning manifest themselves in the $\delta^{15}N$ of the individual NOy compounds. For example, $i_N$RACM predicts that forest conditions will produce $\delta^{15}N$ values in organic nitrate even though there are no isotope effects associated with organic nitrate production or loss in $i_N$RACM. This highlights how the $\delta^{15}N$ values are tracing shifts in $NO_y$ oxidation pathways.

3.3.8 The simulated $\delta^{15}N$ value under the marine conditions

The simulation of $\delta^{15}N$ values of $NO_y$ under the marine conditions is very similar to the forest simulation. The daily oscillations and weekly change in the $\delta^{15}N$ of $NO_x$, HONO and $HNO_3$ all follow the same pattern as the forest simulations but with slight amplification in all compounds. The nighttime change in NO $\delta^{15}N$ is 15‰ (Jan) and 10‰ (June) is about 5‰ larger than in the forest simulation. Similarly, the ocean condition nighttime change in $NO_2$ $\delta^{15}N$ (9 to 12‰) is about 5‰ larger than in the forest simulation. The result is that the $\Delta\delta^{15}N_{NO\text{-}NO2}$ values decrease during the nighttime, reaching minimum values of -13.5‰ (Jan 1) and -3.6‰ (June 1). Again this shows that under low $NO_x$ conditions the $NO_x$ isotopic exchange is not occurring fast enough to reach its full effect ($\varepsilon_{NO/NO2}$ = -35‰ at 298K) and is more pronounced in the summer months due to the short night., relative to the January simulations that have about 14 hours of darkness at this latitude. Similar to the forest simulation the $\delta^{15}N$ values of $HNO_3$ increase stepwise during the daytime and reach the maximum of 16‰ for both the Jan and June simulations. This is about 5‰ larger than in the forest simulation and 15‰ higher than the urban case. Similar to forest simulation, the emission rate of $NO_x$ is higher than the conversion rate of $NO_x$ to $HNO_3$. As a result, the amount of $NO_x$ increases from simulation day 1 to day 5. The abundant $NO_x$ promotes the production of $HNO_3$ during the daytime by $NO_2$ + OH reaction (R39), which leads to the overall increasing trend throughout the simulation period.

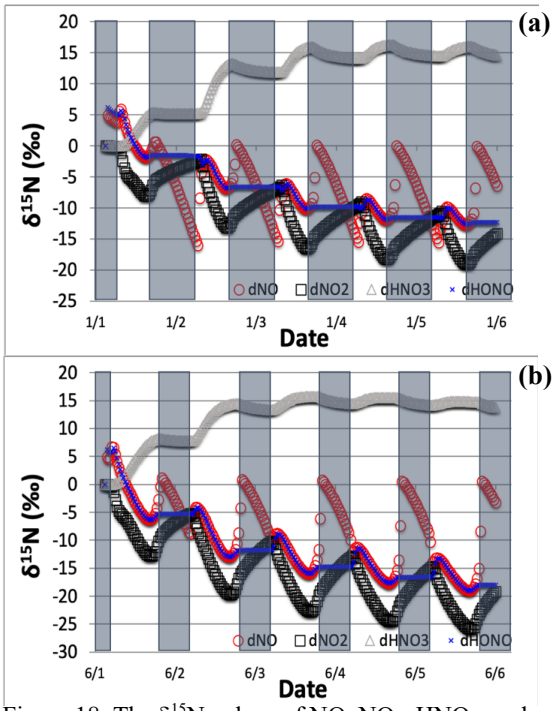

Figure 18. The $\delta^{15}N$ values of NO, $NO_2$, $HNO_3$, and HONO for marine condition for Jan 1 (top, a) and Jun 1 (bottom, b) simulation. The 5-day simulation was under the conditions list in Table S8.

3.4. Model comparison with observations

There are a number of challenges when trying to compare the $i_N$RACM model predictions of $NO_y$ $\delta^{15}N$ values with observations in real world. First, there has yet to be a study where the

https://doi.org/10.5194/gmd-2020-114
Preprint. Discussion started: 22 June 2020



$\delta^{15}N$ values of NO, $NO_2$, and $NO_3^-$ have been simultaneously measured. The most abundant data is on the $\delta^{15}N$ value of $NO_3^-$ in aerosols or rainwater. Even with these studies, a direct comparison is difficult because of the $\delta^{15}N$ value of the source $NO_x$ may be variable in space and time. The $\delta^{15}N$ value of $NO_x$ sources can range from -40 to + 20 ‰ and both $NO_x$ sources and $NO_3^-$ deposition will be a strong function of the transport history of the air mass that is sampled. Without a 3-D chemical transport model that includes the $i_N$RACM mechanism, a direct comparison with most $NO_3^-$ $\delta^{15}N$ studies would be tenuous. In addition, most $NO_y$ $\delta^{15}N$ studies provide neither trace gas concentrations ($NO_x$, $O_3$, CO, VOC) nor local trace gas emissions that would be required to constrain $i_N$RACM for it make an accurate prediction of secondary pollutants or $\delta^{15}N$ values.

The most complete dataset for which to evaluate the $i_N$RACM mechanism is from Riha (2013) in a study in Tucson AZ, USA. In that study $PM_{2.5}$ and $PM_{10}$ were collected weekly (24-hour period) for one year (2006) and the $\delta^{15}N$ value of water soluble $NO_3^-$ was determined (Figure 1). Into PM mass and $NO_3^-$ $\delta^{15}N$ data, local measurements of traces gases (accept VOCs) and meteorology (temperature, relative humidity, wind) were available. In addition, detailed local primary pollutant emission inventories have been developed (Diem and Comrie, 2001). Tucson is a city with little industry or power generation so roughly 80% of the $NO_x$ is due to vehicles and the relative proportion of all NOx sources is invariant throughout the year. Further, Tucson is surrounded by a desert landscape and by and large not influences by regional pollution sources outside the city. These factors overcome some of the uncertainties discussed above. $i_N$RACM was initialized with observed trace gas concentrations and $NO_x$ and VOC emissions were based on previous work (Riha, 2013) and the source $NO_x$ $\delta^{15}N$ value was set to -3‰, typical of vehicle emissions (Walter et al., 2015) and run on the first day of each month. The predicted $NO_3^-$ (as $HNO_3$) $\delta^{15}N$ values (After 48 hours) matched remarkably well with the observed values in $PM_{2.5}$ and $PM_{10}$ (Figure 19). Observed maximums were in the winter months, peaking January at 15‰ close to the model maximum in January of 17%. The minimum $\delta^{15}N$ values (-2‰) are measured in July, similar to model predictions of 0‰ during July. The model captures the

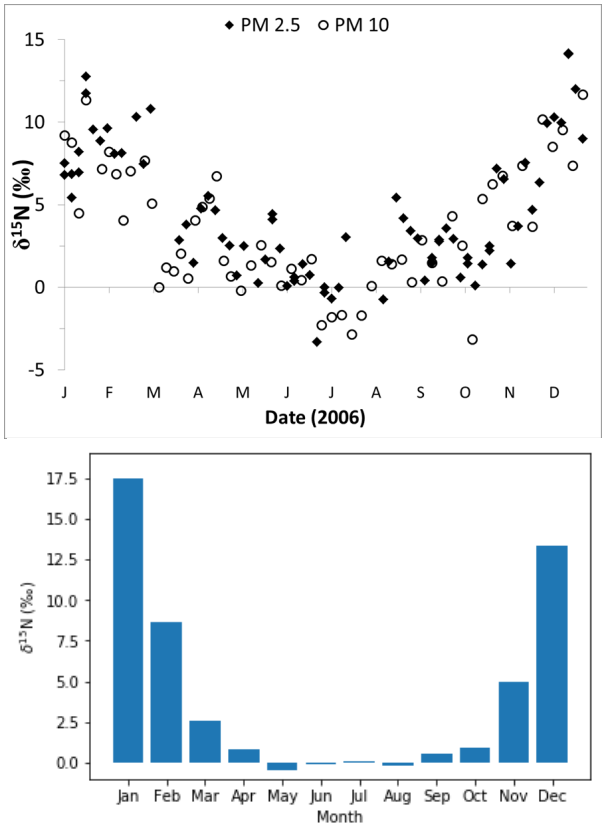


Figure 19. Upper panel is the observed $NO_3^-$ $\delta^{15}N$ values of PM in the city of Tucson (Riha, 2013). Lower panel is the $NO_3^-$ $\delta^{15}N$ values of $HNO_3$ predicted by the $i_N$RACM mechanism. Minimums, maximums, and seasonal change in $\delta^{15}N$ in PM $NO_3^-$ can be explained by the EIE, KIE, and PHIFE occurring during $NO_y$ cycling.

https://doi.org/10.5194/gmd-2020-114
Preprint. Discussion started: 22 June 2020



seasonal trend quite well, including the Spring plateau. This suggests that at this location, the observed seasonal variation in PM $NO_3^-$ $\delta^{15}N$ values can be explained isotope effects associated with the photochemical conversion of NOx into $HNO_3$.

## 4. Conclusion

We have developed the first 0-D photochemical box model for $^{15}N$ compounds in the tropospheric $NO_x$-$NO_y$ cycle. It was shown that of the 100's of N reactions in the RACM mechanism only a handful significantly impact the main $NO_y$ compounds ($NO_x$, HONO, $HNO_3$). Primarily these are Leighton cycle reactions, $NO_2$ + OH, and $NO_x$ isotope exchange, with $N_2O_5$ and nitrate radical reactions having a significant, but minor influence on $NO_y$ $\delta^{15}N$ values. It was also shown that there were two factors that can dramatically influence the simulated $NO_y$ $\delta^{15}N$ values. The first is the size of the isotope fractions factors (KIE, EIE, PHIFE) for any given reaction. For example, the large EIE (assumed) for $NO_2$ + OH was much more important than the small KIE associated with $NO_3$ + VOC reactions. This highlights the need for direct or computational measurements of KIE, EIE, PHIFE in $NO_y$ reactions, particularly R39. The second is that shifts in oxidation pathways caused by pollutant loading are being reflected in the $NO_y$ $\delta^{15}N$ values. In particular, high $NO_x$ + VOC environments with aerosols tend to favor $\delta^{15}N$ that reflects $NO_x$ isotope exchange and $N_2O_5$ uptake, while clean environments favor $\delta^{15}N$ that reflects $NO_x$ cycle and OH oxidation reactions. This highlights that $NO_y$ $\delta^{15}N$ values are not only related to $NO_x$ sources but also affected by $NO_y$ chemistry.

The $i_N$RACM model makes a number of predictions that could be tested by measuring the $\delta^{15}N$ values of various $NO_y$ compounds in different environments and at different temporal scales. First, the model predicts very large diurnal changes in $NO_x$ $\delta^{15}N$ values in all environments, ranging from 10 to 40‰, which could be easily be detected with even the crudest isotope methods (± 2‰). Second, it predicts that in highly polluted environments the $\delta^{15}N$ value of $HNO_3$ will be close to the $\delta^{15}N$ value of the $NO_x$ sources in the area, but in clean environments, it will be 10 to 15‰ heavier. Third, it predicts seasonal and latitudinal trends in $HNO_3$ $\delta^{15}N$ values driven by sunlight and the shifting photochemical pathways associated with it. It predicts higher winter $HNO_3$ $\delta^{15}N$ values, as $NO_x$ isotope exchange becomes more important relative Leighton and OH reactions that become dominant in the summer. This effect should be more pronounced as a function of latitude. There should be relatively minor changes in equatorial $HNO_3$ $\delta^{15}N$ values since sunlight hours do not vary, significant changes at mid-latitudes (50% seasonal sunlight change) change, and essentially a bimodal change at the poles (ignoring snowpack recycling effects). Fourth, it predicts there will be $\delta^{15}N$ variations in key $NO_y$ reservoirs yet to be measured such as organic nitrates and PAN. Finally, the $i_N$RACM model predicts that the most dramatic changes in $NO_y$ $\delta^{15}N$ changes will occur after rain events where $NO_y$ is largely removed from the atmosphere by wet depositions. Post rain, the $NO_y$ $\delta^{15}N$ values effectively "reset", particularly $HNO_3$, and will have their biggest difference relative to the $NO_x$ $\delta^{15}N$ before trending to the $NO_x$ source over time. The $i_N$RACM model suggests that knowing how is $NO_y$ partitioned and the $\delta^{15}N$ value of one (or more) compound that the $\delta^{15}N$ of the $NO_x$ source can be determined. This, in turn, can be used as a constraint on $NO_x$ budgets from the local to regional and global scale.

This effect that tropospheric photochemistry has on $NO_y$ $\delta^{15}N$ values was tested and shown to general initially lead to higher $\delta^{15}N$ values in $HNO_3$ relative to the initial $NO_x$. The difference between the $\delta^{15}N$ of $HNO_3$ relative to the initial (emitted) $NO_x$ was typically ~ +10‰

https://doi.org/10.5194/gmd-2020-114
Preprint. Discussion started: 22 June 2020

Geoscientific Model Development Discussions

by the 2nd and 3rd day of the simulation. This seems consistent with observations that show $NO_3^-$ $\delta^{15}N$ values (positive $\delta^{15}N$) are typically higher than most $NO_x$ sources (negative $\delta^{15}N$). This difference between $NO_x$ source and $HNO_3$ $\delta^{15}N$ values tends to diminish as the simulation progresses as either all of the initial $NO_x$ is oxidized to $HNO_3$ (no emission simulations) or the proportion of $HNO_3$ to total N approaches 1 (emission scenarios). This type of bias can be eliminated by incorporating $i_N$RACM into 3-D chemical transport models that account for time-dependent deposition and emission of $NO_y$.

The model accuracy and its validation could be improved with additional research. The $i_N$RACM model could be refined by additional theoretical and/or experimental determination of the isotope fractionation factors for the N reactions. First and foremost the fractionation factor for the $NO_2$ + OH reaction needs evaluating in a more robust manner. Likewise, the fractionation factor for the NO + OH, another 3-body reaction, will have a large influence on HONO $\delta^{15}N$ values and determining its value will be key for interesting future HONO $\delta^{15}N$ data. The fractionation factor for $NO_2$ photolysis requires attention given the limitation of the ΔZPE PHIFE model [*Blake et al.*, *2003; Liang et al., 2004; Miller and Yung, 2000]*. On the validation end, the simultaneous measurement of $\delta^{15}N$ in multiple $NO_y$ compounds would expose the accuracy or limitations of the $i_N$RACM model in a quantitative way. Repeating these simultaneous measurements in a range of environments would test the predictions made by out test case simulations.

**Code availability**: Fortran code and associated input files are archived on Zenodo.org https://zenodo.org/. DOI/10.5281/zenodo.3834920. An online version of this $i_N$RACM model is available for public use at https://mygeohub.org/tools/sbox/

**Author contribution**: Greg Michalski was the lead investigator for the project designed the modeling experiments, organized the tasks, and wrote the manuscript. Huan Fang and David Mase modified the RACM code to include $^{15}N$ isotopes, assisted in writing and editing the manuscript. Wendell W Walters derived EIE, KIE, and PHIFE used in the model and assisted in writing and editing the paper

**Acknowledgements:** We would like to thank the Purdue Research Foundation and the Purdue Climate Change Research Center for providing funding for the project. We would like to thank Bo Sun for helping with the Fortran coding and data generation.

The authors declare that they have no conflict of interest.

https://doi.org/10.5194/gmd-2020-114
Preprint. Discussion started: 22 June 2020




References

Aldener, M., Brown, S. S., Stark, H., Williams, E. J., Lerner, B. M., Kuster, W. C., ... & Ravishankara, A. R. (2006). Reactivity and loss mechanisms of $NO_3$ and $N_2O_5$ in a polluted marine environment: Results from in situ measurements during New England Air Quality Study 2002. *Journal of Geophysical Research: Atmospheres*, *111*(D23).

Altshuller, A. P. (1989). Nonmethane organic compound to nitrogen oxide ratios and organic composition in cities and rural areas. *JAPCA*, *39*(7), 936-943.

Andreae, M. O., and P. J. Crutzen (1997), Atmospheric aerosols: biogeochemical sources and role in atmospheric chemistry, *Science*, *276*(5315), 1052-1058.

Anttila, T., Kiendler-Scharr, A., Tillmann, R., & Mentel, T. F. (2006). On the reactive uptake of gaseous compounds by organic-coated aqueous aerosols: Theoretical analysis and application to the heterogeneous hydrolysis of $N_2O_5$. *The Journal of Physical Chemistry A*, *110*(35), 10435-10443.

Atkinson, R. (1990), Gas-phase tropospheric chemistry of organic-compounds - a review, *Atmospheric Environment Part a-General Topics*, *24*(1), 1-41, doi:10.1016/0960-1686(90)90438-s.

Atkinson, R. (2000), Atmospheric chemistry of VOCs and $NO_x$, *Atmospheric Environment*, *34*(12-14), 2063-2101.

Atkinson, R., D. L. Baulch, R. A. Cox, R. F. Hampson, J. A. Kerr, and J. Troe (1992), Evaluated kinetic and photochemical data for atmospheric chemistry supplement-iv - IUPAC subcommittee on gas kinetic data evaluation for atmospheric chemistry, *Journal of Physical and Chemical Reference Data*, *21*(6), 1125-1568, doi:10.1063/1.555918.

Bauer, S. E., D. Koch, N. Unger, S. M. Metzger, D. T. Shindell, and D. G. Streets (2007), Nitrate aerosols today and in 2030: a global simulation including aerosols and tropospheric ozone, *Atmospheric Chemistry and Physics*, *7*(19), 5043-5059

Baugues, K. (1986). *Review of NMOC, NOx and NMOC/NOx ratios measured in 1984 and 1985* (No. PB-87-166963/XAB; EPA-450/4-86/015). Environmental Protection Agency, Research Triangle Park, NC (USA). Monitoring and Data Analysis Div..

Bertram, T. H., & Thornton, J. A. (2009). Toward a general parameterization of $N_2O_5$ reactivity on aqueous particles: the competing effects of particle liquid water, nitrate and chloride. *Atmospheric Chemistry and Physics*, *9*(21), 8351-8363.

Bigeleisen, J. (1958), Second-Order Sum Rule for the Vibrations of Isotopic Molecules and the Second Rule of the Mean, *The Journal of Chemical Physics*, *28*(4), 694-699.

Bigeleisen, J., and M. G. Mayer (1947), Calculation of Equilibrium Constants for Isotopic Exchange Reactions, *The Journal of Chemical Physics*, *15*(5), 261-267.

https://doi.org/10.5194/gmd-2020-114
Preprint. Discussion started: 22 June 2020




Bigeleisen, J., and M. Wolfsberg (1958), Theoretical and experimental aspects of isotope effects in chemical kinetics, *Advances in Chem. Phys. (Prigogine, I. Interscience Publishers, Inc. , New York)*, *1*, 15-76.

Blake, G. A., M. C. Liang, C. G. Morgan, and Y. L. Yung (2003), A born-oppenheimer photolysis model of $N_2O$ fractionation, *Geophysical Research Letters*, *30*(12), 58/51-58/54.

Bloss, W. J., M. J. Evans, J. D. Lee, R. Sommariva, D. E. Heard, and M. J. Pilling (2005), The oxidative capacity of the troposphere: Coupling of field measurements of OH and a global chemistry transport model, *Faraday Discussions*, *130*, 425-436.

Bottenheim, J. W., Gallant, A. G., & Brice, K. A. (1986). Measurements of NOy species and O3 at 82 N latitude. *Geophysical Research Letters*, *13*(2), 113-116.

Brimblecombe, P., H. Hara, and D. Houle (2007), *Acid Rain - Deposition to Recovery*, Springer.

Brown, P. N., G. D. Byrne, and A. C. Hindmarsh (1989), VODE - A variable-coefficient ode solver, *Siam Journal on Scientific and Statistical Computing*, *10*(5), 1038-1051, doi:10.1137/0910062.

Hindmarsh, A. C. (1983), ODEPACK, a systematized collection of ODE solvers, in *IMACS Transactions on Scientific Computation*, edited by R.S. Stepleman, M. Carver, R. Peskin, W.F. Ames, R. Vichnevetsky, pp. 55-64, Amsterdam.

Brown, S. S., J. B. Burkholder, R. K. Talukdar, and A. R. Ravishankara (2001), Reaction of hydroxyl radical with nitric acid: insights into its mechanism, *Journal of Physical Chemistry A*, *105*(9), 1605-1614.

Brown, L. L., & Begun, G. M. (1959). Nitrogen isotopic fractionation between nitric acid and the oxides of nitrogen. *The Journal of Chemical Physics*, *30*(5), 1206-1209.

Brown, S. S., et al. (2006), Variability in nocturnal nitrogen oxide processing and its role in regional air quality, *Science*, *311*(5757), 67-70.

Bruningfann, C. S., and J. B. Kaneene (1993), The Effects of Nitrate, Nitrite and N-Nitroso Compounds on Human Health - A Review, *Veterinary and Human Toxicology*, *35*(6), 521-538.

Carroll, M. A., Ridley, B. A., Montzka, D. D., Hubler, G., Walega, J. G., Norton, R. B., ... & Grahek, F. E. (1992). Measurements of nitric oxide and nitrogen dioxide during the Mauna Loa Observatory Photochemistry Experiment. *Journal of Geophysical Research: Atmospheres*, *97*(D10), 10361-10374.

Cao, Z. Y., X. H. Zhou, Y. J. Ma, L. P. Wang, R. D. Wu, B. Chen, and W. X. Wang (2017), The Concentrations, Formations, Relationships and Modeling of Sulfate, Nitrate and Ammonium

https://doi.org/10.5194/gmd-2020-114
Preprint. Discussion started: 22 June 2020




(SNA) Aerosols over China, *Aerosol and Air Quality Research*, *17*(1), 84-97, doi:10.4209/aaqr.2016.01.0020.

Chai, J. J., and M. G. Hastings (2018), Collection Method for Isotopic Analysis of Gaseous Nitrous Acid, *Analytical Chemistry*, *90*(1), 830-838, doi:10.1021/acs.analchem.7b03561.

Chang, W. L., P. V. Bhave, S. S. Brown, N. Riemer, J. Stutz, and D. Dabdub (2011), Heterogeneous Atmospheric Chemistry, Ambient Measurements, and Model Calculations of $N_2O_5$: A Review, *Aerosol Science and Technology*, *45*(6), 665-695.

Charlson, R. J., S. E. Schwartz, J. M. Hales, R. D. Cess, J. A. Coakley, J. E. Hansen, and D. J. Hofmann (1992), Climate Forcing by Anthropogenic Aerosols, *Science*, *255*(5043), 423-430.

Chen, W. T., H. Liao, and J. H. Seinfeld (2007), Future climate impacts of direct radiative forcing of anthropogenic aerosols, tropospheric ozone, and long-lived greenhouse gases, *Journal of Geophysical Research-Atmospheres*, *112*(D14).

Cleveland, W. S., Kleiner, B., McRae, J. E., Warner, J. L., & Pasceri, R. E. (1977). Geographical properties of ozone concentrations in the northeastern United States. *Journal of the Air Pollution Control Association*, *27*(4), 325-328.

Cooper, O. R., Gao, R. S., Tarasick, D., Leblanc, T., & Sweeney, C. (2012). Long-term ozone trends at rural ozone monitoring sites across the United States, 1990–2010. *Journal of Geophysical Research: Atmospheres*, *117*(D22).

Davis, J. M., Bhave, P. V., & Foley, K. M. (2008). Parameterization of $N_2O_5$ reaction probabilities on the surface of particles containing ammonium, sulfate, and nitrate. *Atmospheric Chemistry and Physics*, *8*(17), 5295-5311.

Day, D. A., M. B. Dillon, P. J. Wooldridge, J. A. Thornton, R. S. Rosen, E. C. Wood, and R. C. Cohen (2003), On alkyl nitrates, $O_3$, and the "missing $NO_y$", *Journal of Geophysical Research-Atmospheres*, *108*(D16), doi:10.1029/2003jd003685.

DeMore, W. B., S. P. Sander,D. M. Golden, R. F. Hampson,M. J. Kurylo, C. J. Howard, A. R. Ravishankara,C. E. Kolb, and M. J. Molina, (1994), Chemical kinetics and photochemical data for use in stratospheric modeling, Eval. 11, *Natl. Aeronaut. and Space Admin., Jet Propul. Lab.*

Dentener, F. J., and P. J. Crutzen (1993), Reaction of nitrogen pentoxide on tropospheric aerosols: Impact on the global distributions of $NO_x$, ozone, and hydroxyl, *Journal of Geophysical Research*, *98*(D4), 7149-7163.

Diem, J. E., & Comrie, A. C. (2001). Allocating anthropogenic pollutant emissions over space: application to ozone pollution management. *Journal of environmental management*, *63*(4), 425-447.

https://doi.org/10.5194/gmd-2020-114
Preprint. Discussion started: 22 June 2020




Du, E. Z., M. E. Fenn, W. De Vries, and Y. S. Ok (2019), Atmospheric nitrogen deposition to global forests: Status, impacts and management options, *Environmental Pollution*, *250*, 1044-1048, doi:10.1016/j.envpol.2019.04.014.

Elliott, E. M., C. Kendall, E. W. Boyer, D. A. Burns, G. G. Lear, H. E. Golden, K. Harlin, A. Bytnerowicz, T. J. Butler, and R. Glatz (2009), Dual nitrate isotopes in dry deposition: Utility for partitioning $NO_x$ source contributions to landscape nitrogen deposition, *Journal of Geophysical Research-Biogeosciences*, *114*.

Elliott, E. M., C. Kendall, S. D. Wankel, D. A. Burns, E. W. Boyer, K. Harlin, D. J. Bain, and T. J. Butler (2007), Nitrogen isotopes as indicators of NOx source contributions to atmospheric nitrate deposition across the Midwestern and northeastern United States, *Environmental Science & Technology*, *41*(22), 7661-7667.

Elliott, E. M., Z. J. Yu, A. S. Cole, and J. G. Coughlin (2019), Isotopic advances in understanding reactive nitrogen deposition and atmospheric processing, *Science of the Total Environment*, *662*, 393-403, doi:10.1016/j.scitotenv.2018.12.177.

Fahey, D. W., Hübler, G., Parrish, D. D., Williams, E. J., Norton, R. B., Ridley, B. A., ... & Fehsenfeld, F. C. (1986). Reactive nitrogen species in the troposphere: Measurements of NO, $NO_2$, $HNO_3$, particulate nitrate, peroxyacetyl nitrate (PAN), $O_3$, and total reactive odd nitrogen ($NO_y$) at Niwot Ridge, Colorado. *Journal of Geophysical Research: Atmospheres*, *91*(D9), 9781-9793.

Felix, J. D., and E. M. Elliott (2014), Isotopic composition of passively collected nitrogen dioxide emissions: Vehicle, soil and livestock source signatures, *Atmospheric Environment*, *92*, 359-366, doi:10.1016/j.atmosenv.2014.04.005.

Felix, J. D., E. M. Elliott, and S. L. Shaw (2012), Nitrogen Isotopic Composition of Coal-Fired Power Plant $NO_x$: Influence of Emission Controls and Implications for Global Emission Inventories, *Environmental Science & Technology*, *46*(6), 3528-3535.

Felix, J. D., Elliott, E. M., Avery, G. B., Kieber, R. J., Mead, R. N., Willey, J. D., & Mullaugh, K. M. (2015). Isotopic composition of nitrate in sequential Hurricane Irene precipitation samples: implications for changing $NO_x$ sources. *Atmospheric Environment*, *106*, 191-195.

Fibiger, D. L., and M. G. Hastings (2016), First Measurements of the Nitrogen Isotopic Composition of $NO_x$ from Biomass Burning, *Environmental Science & Technology*, *50*(21), 11569-11574, doi:10.1021/acs.est.6b03510.

Finlayson-Pitts, B. J., and J. N. Pitts, Jr. (2000), *Chemistry of the Upper and Lower Atmosphere*, Academic Press, San Diego.

Fowler, D., et al. (2013), The global nitrogen cycle in the twenty-first century, *Philosophical Transactions of the Royal Society B-Biological Sciences*, *368*(1621).

https://doi.org/10.5194/gmd-2020-114
Preprint. Discussion started: 22 June 2020




Freyer, H. D. (1978), Seasonal Trends of $NH_4^+$ and $NO_3^-$ Nitrogen Isotope Composition in Rain Collected at Julich, Germany, *Tellus*, *30*(1), 83-92.

Freyer, H. D., D. Kley, A. Volzthomas, and K. Kobel (1993), On the interaction of isotopic exchange processes with photochemical-reactions in atmospheric oxides of nitrogen, *Journal of Geophysical Research-Atmospheres*, *98*(D8), 14791-14796, doi:10.1029/93jd00874.
for Global Emission Inventories, *Environmental Science & Technology*, *46*(6), 3528-3535.

Freyer, H. D., D. Kley, A. Volzthomas, and K. Kobel (1993), On the interaction of isotopic exchange processes with photochemical-reactions in atmospheric oxides of nitrogen, *Journal of Geophysical Research-Atmospheres*, *98*(D8), 14791-14796, doi:10.1029/93jd00874.

Fuentes, J. D., Chamecki, M., Nascimento dos Santos, R. M., Von Randow, C., Stoy, P. C., Katul, G., ... & Souza Freire, L. (2016). Linking meteorology, turbulence, and air chemistry in the Amazon rain forest. *Bulletin of the American Meteorological Society*, *97*(12), 2329-2342.

Galloway, J. N., Dentener, F. J., Capone, D. G., Boyer, E. W., Howarth, R. W., Seitzinger, S. P., . & Karl, D. M. (2004). Nitrogen cycles: past, present, and future. *Biogeochemistry*, *70*(2), 153-226.

Golden, D. M., and G. P. Smith (2000), Reaction of OH + $NO_2$ + M: A new view, *Journal of Physical Chemistry A*, *104*(17), 3991-3997.

Greenberg, J. P., & Zimmerman, P. R. (1984). Nonmethane hydrocarbons in remote tropical, continental, and marine atmospheres. *Journal of Geophysical Research: Atmospheres*, *89*(D3), 4767-4778.

Gregory, G. L., Browell, E. V., & Warren, L. S. (1988). Boundary layer ozone: An airborne survey above the Amazon Basin. *Journal of Geophysical Research: Atmospheres*, *93*(D2), 1452-1468.

Hall, J. V., A. M. Winer, M. T. Klienman, F. W. Lurmann, V. Brajer, and S. D. Colome (1992), Valuing the Health Benefits of Clean Air, *Science*, *V255*, 812-817.

Hagenbjörk, A., Malmqvist, E., Mattisson, K., Sommar, N. J., & Modig, L. (2017). The spatial variation of $O_3$, NO, $NO_2$ and $NO_x$ and the relation between them in two Swedish cities. *Environmental monitoring and assessment*, *189*(4), 161.

Harrison, R. M., J. L. Grenfell, S. Yamulki, K. C. Clemitshaw, S. A. Penkett, J. N. Cape, and G. G. McFadyen (1999), Budget of $NO_y$ species measured at a coastal site, *Atmospheric Environment*, *33*(26), 4255-4272, doi:10.1016/s1352-2310(99)00176-4.

Hastings, M. G., K. L. Casciotti, and E. M. Elliott (2013), Stable Isotopes as Tracers of Anthropogenic Nitrogen Sources, Deposition, and Impacts, *Elements*, *9*(5), 339-344.

Hastings, M. G., Sigman, D. M., & Lipschultz, F. (2003). Isotopic evidence for source changes of nitrate in rain at Bermuda. *Journal of Geophysical Research: Atmospheres*, *108*(D24).

https://doi.org/10.5194/gmd-2020-114
Preprint. Discussion started: 22 June 2020




He, H., Stehr, J. W., Hains, J. C., Krask, D. J., Doddridge, B. G., Vinnikov, K. Y., ... & Dickerson, R. R. (2013). Trends in emissions and concentrations of air pollutants in the lower troposphere in the Baltimore/Washington airshed from 1997 to 2011. *Atmospheric Chemistry and Physics*, *13*(15), 7859-7874.

Heaton, T. H. E. (1987). 15N 14N ratios of nitrate and ammonium in rain at Pretoria, South Africa. *Atmospheric Environment (1967)*, *21*(4), 843-852.

Hegglin, M. I., D. Brunner, T. Peter, P. Hoor, H. Fischer, J. Staehelin, M. Krebsbach, C. Schiller, U. Parchatka, and U. Weers (2006), Measurements of NO, $NO_y$, $N_2O$, and $O_3$ during SPURT: implications for transport and chemistry in the lowermost stratosphere, *Atmospheric Chemistry and Physics*, *6*, 1331-1350, doi:10.5194/acp-6-1331-2006.

Horowitz, L. W., J. Liang, G. M. Gardner, and D. J. Jacob (1998), Export of reactive nitrogen from North America during summertime: sensitivity to hydrocarbon chemistry, *Journal of Geophysical Research*, *103*(D11), 13451-13476.

Houlton, B. Z., Boyer, E., Finzi, A., Galloway, J., Leach, A., Liptzin, D., ... & Townsend, A. R. (2013). Intentional versus unintentional nitrogen use in the United States: trends, efficiency and implications. *Biogeochemistry*, *114*(1-3), 11-23.

Hoyle, C. R., et al. (2011), A review of the anthropogenic influence on biogenic secondary organic aerosol, *Atmospheric Chemistry and Physics*, *11*(1), 321-343, doi:10.5194/acp-11-321-2011.

Hudman, R. C., Moore, N. E., Mebust, A. K., Martin, R. V., Russell, A. R., Valin, L. C., & Cohen, R. C. (2012). Steps towards a mechanistic model of global soil nitric oxide emissions: implementation and space based-constraints. *Atmospheric Chemistry and Physics*, *12*(16), 7779-7795.

Jaffe, D. A., Honrath, R. E., Zhang, L., Akimoto, H., Shimizu, A., Mukai, H., ... & Merrill, J. (1996). Measurements of NO, $NO_y$, CO and $O_3$ and estimation of the ozone production rate at Oki Island, Japan, during PEM-West. *Journal of Geophysical Research: Atmospheres*, *101*(D1), 2037-2048.

Janach, W. E. (1989). Surface ozone: trend details, seasonal variations, and interpretation. *Journal of Geophysical Research: Atmospheres*, *94*(D15), 18289-18295.
Kirchhoff, V. W. (1988). Surface ozone measurements in Amazonia. *Journal of Geophysical Research: Atmospheres*, *93*(D2), 1469-1476.

Kastler, J., & Ballschmiter, K. (1998). Bifunctional alkyl nitrates–trace constituents of the atmosphere. *Fresenius' journal of analytical chemistry*, *360*(7-8), 812-816.

https://doi.org/10.5194/gmd-2020-114
Preprint. Discussion started: 22 June 2020




Kuang, C., Riipinen, I., Sihto, S. L., Kulmala, M., McCormick, A. V., & McMurry, P. H. (2010). An improved criterion for new particle formation in diverse atmospheric environments. *Atmospheric Chemistry and Physics*, *10*(17), 8469-8480.

Lajtha, K., and J. Jones (2013), Trends in cation, nitrogen, sulfate and hydrogen ion concentrations in precipitation in the United States and Europe from 1978 to 2010: a new look at an old problem, *Biogeochemistry*, *116*(1-3), 303-334, doi:10.1007/s10533-013-9860-2.
Lelieveld, J., et al. (2008), Atmospheric oxidation capacity sustained by a tropical forest, *Nature*, *452*(7188), 737-740.

Lee, S. H., Uin, J., Guenther, A. B., de Gouw, J. A., Yu, F., Nadykto, A. B., ... & Baumann, K. (2016). Isoprene suppression of new particle formation: Potential mechanisms and implications. *Journal of Geophysical Research: Atmospheres*, *121*(24), 14-621.

Lefohn, A. S., & Pinkerton, J. E. (1988). High resolution characterization of ozone data for sites located in forested areas of the United States. *JAPCA*, *38*(12), 1504-1511.

Liang, M. C., G. A. Blake, and Y. L. Yung (2004), A semianalytic model for photo-induced isotopic fractionation in simple molecules, *Journal of Geophysical Research-Atmospheres*, *109*(D10).

Logan, J. A. (1989). Ozone in rural areas of the United States. *Journal of Geophysical Research: Atmospheres*, *94*(D6), 8511-8532.

Ma, J. Z., Y. C. Liu, C. Han, Q. X. Ma, C. Liu, and H. He (2013), Review of heterogeneous photochemical reactions of NOy on aerosol - A possible daytime source of nitrous acid (HONO) in the atmosphere, *Journal of Environmental Sciences-China*, *25*(2), 326-334, doi:10.1016/s1001-0742(12)60093-x.

Ma, Z., Liu, C., Zhang, C., Liu, P., Ye, C., Xue, C., ... & Mu, Y. (2019). The levels, sources and reactivity of volatile organic compounds in a typical urban area of Northeast China. *Journal of Environmental Sciences*, *79*, 121-134.

Madronich, S. (1987). Photodissociation in the atmosphere: 1. Actinic flux and the effects of ground reflections and clouds. *Journal of Geophysical Research: Atmospheres*, *92*(D8), 9740-9752.

McMurry, P. H., Fink, M., Sakurai, H., Stolzenburg, M. R., Mauldin III, R. L., Smith, J., ... & Huey, L. G. (2005). A criterion for new particle formation in the sulfur-rich Atlanta atmosphere. *Journal of Geophysical Research: Atmospheres*, *110*(D22).

Michalski, G., R. Jost, D. Sugny, M. Joyeux, and M. Thiemens (2004), Dissociation energies of six $NO_2$ isotopologues by laser induced fluorescence and zero point energy of some triatomic molecules *Journal of Chemical Physics*, *121*(15), 7153-7161.

Miller, C. E., and Y. L. Yung (2000), Photo-induced isotopic fractionation, *Journal of Geophysical Research-Atmospheres*, *105*(D23), 29039-29051.

https://doi.org/10.5194/gmd-2020-114
Preprint. Discussion started: 22 June 2020




Morino, Y., Y. Kondo, N. Takegawa, Y. Miyazaki, K. Kita, Y. Komazaki, M. Fukuda, T. Miyakawa, N. Moteki, and D. R. Worsnop (2006), Partitioning of $HNO_3$ and particulate nitrate over Tokyo: Effect of vertical mixing, *Journal of Geophysical Research-Atmospheres*, *111*(D15), doi:10.1029/2005jd006887.

Moore, H. (1977). The isotopic composition of ammonia, nitrogen dioxide and nitrate in the atmosphere. *Atmospheric Environment (1967)*, *11*(12), 1239-1243.

National Research Council. (1992). *Rethinking the ozone problem in urban and regional air pollution*. National Academies Press.

Pan, Y. P., S. L. Tian, D. W. Liu, Y. T. Fang, X. Y. Zhu, M. Gao, G. R. Wentworth, G. Michalski, X. J. Huang, and Y. S. Wang (2018), Source Apportionment of Aerosol Ammonium in an Ammonia-Rich Atmosphere: An Isotopic Study of Summer Clean and Hazy Days in Urban Beijing, *Journal of Geophysical Research-Atmospheres*, *123*(10), 5681-5689, doi:10.1029/2017jd028095.

Parrish, D. D., Trainer, M., Williams, E. J., Fahey, D. W., Hübler, G., Eubank, C. S., ... & Fehsenfeld, F. C. (1986). Measurements of the $NO_x$-$O_3$ photostationary state at Niwot Ridge, Colorado. *Journal of Geophysical Research: Atmospheres*, *91*(D5), 5361-5370.

Paulot, F., P. Ginoux, W. F. Cooke, L. J. Donner, S. Fan, M. Y. Lin, J. Mao, V. Naik, and L. W. Horowitz (2016), Sensitivity of nitrate aerosols to ammonia emissions and to nitrate chemistry: implications for present and future nitrate optical depth, *Atmospheric Chemistry and Physics*, *16*(3), 1459-1477, doi:10.5194/acp-16-1459-2016.

Petäjä, T., Mauldin Iii, R. L., Kosciuch, E., McGrath, J., Nieminen, T., Paasonen, P., ... & Kulmala, M. (2009). Sulfuric acid and OH concentrations in a boreal forest site. *Atmospheric Chemistry and Physics*, *9*(19), 7435-7448.

Pilegaard, K. (2013). Processes regulating nitric oxide emissions from soils. *Phil. Trans. R. Soc. B*, *368*(1621), 20130126

Platt, U. F., A. M. Winer, H. W. Biermann, R. Atkinson, and J. N. Pitts (1984), Measurement of Nitrate Radical Concentrations in Continental Air, *Environmental Science & Technology*, *18*(5), 365-369.

Prinn, R. G. (2003), The cleansing capacity of the atmosphere, *Annual Review of Environment and Resources*, *28*, 29-57.

Pusede, S. E., et al. (2016), On the effectiveness of nitrogen oxide reductions as a control over ammonium nitrate aerosol, *Atmospheric Chemistry and Physics*, *16*(4), 2575-2596, doi:10.5194/acp-16-2575-2016.

Pye, H. O. T., A. W. H. Chan, M. P. Barkley, and J. H. Seinfeld (2010), Global modeling of organic aerosol: the importance of reactive nitrogen ($NO_x$ and $NO_3$), *Atmospheric Chemistry and Physics*, *10*(22), 11261-11276.

https://doi.org/10.5194/gmd-2020-114
Preprint. Discussion started: 22 June 2020




Qi, X. M., Ding, A. J., Nie, W., Petäjä, T., Kerminen, V. M., Herrmann, E., and Sun, J. N. (2015). Aerosol size distribution and new particle formation in the western Yangtze River Delta of China: 2 years of measurements at the SORPES station. *Atmospheric chemistry and physics*, *15*(21), 12445-12464.

Richet, P., Y. Bottinga, and M. Javoy (1977), Review of hydrogen, carbon, nitrogen, oxygen, sulfur, and chlorine stable isotope fractionation among gaseous molecules, *Annual Review of Earth and Planetary Sciences*, *5*, 65-110

Riemer, N., Vogel, H., Vogel, B., Anttila, T., Kiendler-Scharr, A., and Mentel, T. F. (2009). Relative importance of organic coatings for the heterogeneous hydrolysis of $N_2O_5$ during summer in Europe. *Journal of Geophysical Research: Atmospheres*, *114*(D17).

Riemer, N., H. Vogel, B. Vogel, B. Schell, I. Ackermann, C. Kessler, and H. Hass (2003), Impact of the heterogeneous hydrolysis of $N_2O_5$ on chemistry and nitrate aerosol formation in the lower troposphere under photosmog conditions, *Journal of Geophysical Research*, *108*(D4), 4144-DOI: 4110.1029/2002JD002436.

Riha, K. M. (2013). The use of stable isotopes to constrain the nitrogen cycle. Purdue University, West Lafayette, IN

Roehl, C. M., J. J. Orlando, G. S. Tyndall, R. E. Shetter, G. J. Vazquez, C. A. Cantrell, and J. G. Calvert (1994), Temperature-dependence of the quantum yields for the photolysis of $NO_2$ near the dissociation limit, *Journal of Physical Chemistry*, *98*(32), 7837-7843, doi:10.1021/j100083a015.

Romer, P. S., Duffey, K. C., Wooldridge, P. J., Allen, H. M., Ayres, B. R., Brown, S. S., ... & Feiner, P. A. (2016). The lifetime of nitrogen oxides in an isoprene-dominated forest. *Atmospheric Chemistry and Physics*, *16*(12), 7623-7637.

Saito, T., Yokouchi, Y., & Kawamura, K. (2000). Distributions of $C^2$–$C^6$ hydrocarbons over the western North Pacific and eastern Indian Ocean. *Atmospheric environment*, *34*(25), 4373-4381.

Savard, M. M., Cole, A., Smirnoff, A., & Vet, R. (2017). δ15N values of atmospheric N species simultaneously collected using sector-based samplers distant from sources–Isotopic inheritance and fractionation. *Atmospheric environment*, *162*, 11-22.

Sharma, H. D., R. E. Jervis, and K. Y. Wong (1970), Isotopic exchange reactions in nitrogen oxides, *Journal of Physical Chemistry*, *74*(4), 923-933.

Shepherd, M. F., Barzetti, S., & Hastie, D. R. (1991). The Production of Atmospheric $NO_2$ and $N_2O$ from a Fertilized Agricultural Soil.

https://doi.org/10.5194/gmd-2020-114
Preprint. Discussion started: 22 June 2020




Shrivastava, M., Cappa, C. D., Fan, J., Goldstein, A. H., Guenther, A. B., Jimenez, J. L., ... & Petaja, T. (2017). Recent advances in understanding secondary organic aerosol: Implications for global climate forcing. *Reviews of Geophysics*, *55*(2), 509-559.

Sjostedt, S. J., Slowik, J. G., Brook, J. R., Chang, R. W., Mihele, C., Stroud, C. A., ... & Abbatt, J. P. D. (2011). Diurnally resolved particulate and VOC measurements at a rural site: indication of significant biogenic secondary organic aerosol formation. *Atmospheric Chemistry and Physics*, *11*(12), 5745-5760.

Snyder, J. A., D. Hanway, J. Mendez, A. J. Jamka, and F. M. Tao (1999), A density functional theory study of the gas-phase hydrolysis of dinitrogen pentoxide, *Journal of Physical Chemistry A*, *103*(46), 9355-9358.

Spak, S. N., and T. Holloway (2009), Seasonality of speciated aerosol transport over the Great Lakes region, *Journal of Geophysical Research-Atmospheres*, *114*.

Srivastava, R. K., Neuffer, W., Grano, D., Khan, S., Staudt, J. E., & Jozewicz, W. (2005). Controlling $NO_x$ emission from industrial sources. *Environmental progress*, *24*(2), 181-197.

Seinfeld, J. H., and S. N. Pandis (1998), *Atmospheric chemistry and physics : from air pollution to climate change*, 1 ed., New York : Wiley.

Stockwell, W. R., F. Kirchner, M. Kuhn, and S. Seefeld (1997), A new mechanism for regional atmospheric chemistry modeling, *Journal of Geophysical Research*, *102*(D22), 25847-25879.

Stockwell, W. R., P. Middleton, J. S. Chang, and X. Y. Tang (1990), The 2nd Generation Regional Acid Deposition Model Chemical Mechanism for Regional Air-Quality Modeling, *Journal of Geophysical Research-Atmospheres*, *95*(D10), 16343-16367.

Torres, A. L., & Buchan, H. (1988). Tropospheric nitric oxide measurements over the Amazon Basin. *Journal of Geophysical Research: Atmospheres*, *93*(D2), 1396-1406.

Urey, H. C. (1947), Thermodynamic properties of isotopic substances, *J. Chem. Soc*, 562-581.

Van Hook, W. A., L. P. N. Rebelo, and M. Wolfsberg (2001), An interpretation of the vapor phase second virial coefficient isotope effect: Correlation of virial coefficient and vapor pressure isotope effects, *Journal of Physical Chemistry A*, *105*(40), 9284-9297, doi:10.1021/jp004305z.

Vandaele, A. C., C. Hermans, S. Fally, M. Carleer, R. Colin, M. F. Merienne, A. Jenouvrier, and B. Coquart (2002), High-resolution Fourier transform measurement of the $NO_2$ visible and near-infrared absorption cross sections: Temperature and pressure effects, *Journal of Geophysical Research-Atmospheres*, *107*(D18), doi:10.1029/2001jd000971.

Walters, W., S. Goodwin, Michalski, and G. (2015a), Nitrogen Stable Isotope Composition of Vehile Emitted $NO_x$, *Environemental Science and Technology*, *49*(4), 2278-2285.

https://doi.org/10.5194/gmd-2020-114
Preprint. Discussion started: 22 June 2020




Walters, W. W., H. Fang, and G. Michalski (2018), Summertime diurnal variations in the isotopic composition of atmospheric nitrogen dioxide at a small midwestern United States city, *Atmospheric Environment*, *179*, 1-11, doi:10.1016/j.atmosenv.2018.01.047.

Walters, W. W., and G. Michalski (2015), Theoretical calculation of nitrogen isotope equilibrium exchange fractionation factors for various $NO_y$ molecules, *Geochimica Et Cosmochimica Acta*, *164*, 284-297, doi:10.1016/j.gca.2015.05.029.

Walters, W. W., and G. Michalski (2016), Ab initio study of nitrogen and position-specific oxygen kinetic isotope effects in the NO + $O_3$ reaction, *Journal of Chemical Physics*, *145*(22), doi:10.1063/1.4968562.

Walters, W. W., D. S. Simonini, and G. Michalski (2016), Nitrogen isotope exchange between NO and $NO_2$ and its implications for $^{15}N$ variations in tropospheric $NO_x$ and atmospheric nitrate, *Geophysical Research Letters*, *43*(1), 440-448, doi:10.1002/2015gl066438.

Walters, W. W., B. D. Tharp, H. Fang, B. J. Kozak, and G. Michalski (2015b), Nitrogen Isotope Composition of Thermally Produced NOx from Various Fossil-Fuel Combustion Sources, *Environmental Science & Technology*, *49*(19), 11363-11371, doi:10.1021/acs.est.5b02769.

Wang, T., Xue, L., Brimblecombe, P., Lam, Y. F., Li, L., & Zhang, L. (2017). Ozone pollution in China: A review of concentrations, meteorological influences, chemical precursors, and effects. *Science of the Total Environment*, *575*, 1582-1596.

Williams, E. J., Parrish, D. D., & Fehsenfeld, F. C. (1987). Determination of nitrogen oxide emissions from soils: Results from a grassland site in Colorado, United States. *Journal of Geophysical Research: Atmospheres*, *92*(D2), 2173-2179.

Wolfsberg, M. (1960), Note on secondary isotope effects in reaction rates, *Journal of Chemical Physics*, *33*(1), 2-6, doi:10.1063/1.1731078.

Wolfsberg, M., W. A. Van Hook, P. Paneth, L. P. N. Rebelo, M. Wolfsberg, W. A. VanHook, and P. Paneth (2010), *Isotope Effects on Equilibrium Constants of Chemical Reactions; Transition State Theory of Isotope Effects*, 77-137 pp., doi:10.1007/978-90-481-2265-3_4.

Yang, J., Honrath, R. E., Peterson, M. C., Parrish, D. D., & Warshawsky, M. (2004). Photostationary state deviation–estimated peroxy radicals and their implications for $HO_x$ and ozone photochemistry at a remote northern Atlantic coastal site. *Journal of Geophysical Research: Atmospheres*, *109*(D2).

Yu, Z., & Elliott, E. M. (2017). Novel method for nitrogen isotopic analysis of soil-emitted nitric oxide. *Environmental Science & Technology*, *51*(11), 6268-6278.

Zhang, Y., K. Vijayaraghavan, X. Y. Wen, H. E. Snell, and M. Z. Jacobson (2009), Probing into regional ozone and particulate matter pollution in the United States: 1. A 1 year CMAQ simulation and evaluation using surface and satellite data, *Journal of Geophysical Research-Atmospheres*, *114*.

https://doi.org/10.5194/gmd-2020-114
Preprint. Discussion started: 22 June 2020


Geoscientific Model Development Discussions
Open Access

Zimmerman, P. R., Greenberg, J. P., & Westberg, C. E. (1988). Measurements of atmospheric hydrocarbons and biogenic emission fluxes in the Amazon boundary layer. *Journal of Geophysical Research: Atmospheres*, *93*(D2), 1407-1416.